This is a preprint, the final version is subject to change, of the American Mineralogist (MSA)
Cite as Authors (Year) Title. American Mineralogist, in press.
(DOI will not work until issue is live.) DOI: http://dx.doi.org/10.2138/am-2017-5716

Manuscript 5716, 1st revision

Fluids and trace element transport in subduction zones

HANS KEPPLER

Bayerisches Geoinstitut, Universität Bayreuth, 95440 Bayreuth, Germany

hans.keppler@uni-bayreuth.de

ABSTRACT

Melt inclusion data from primitive arc basalts from Mexico and Kamchatka show clear positive correlations of "fluid mobile element" / H_2O ratios with the Cl/H_2O ratio, suggesting that the trace element content of subduction zone fluids is strongly enhanced by complexing with chloride. This effect is observed for large-ion lithophile (LILE) elements, (e.g. Rb and Sr), but also for the light rare earth elements (REE, e.g. La and Ce) as well as for U. The correlations of these elements with Cl/H_2O cannot be explained by the addition of sediment melts or slab melts to the mantle source, since Cl has no effect on the solubility or partitioning of these elements in silicate melt systems. On the other hand, the observed relationship of trace element abundance with Cl is consistent with a large body of experimental data showing greatly enhanced partitioning into aqueous fluid upon addition of chloride. Accordingly, it appears that a rather dilute, Cl-bearing aqueous fluid is the main carrier of LILE, light REE, and U from the slab to the source of melting in arcs. Moreover, elevated Ce/H_2O ratios clearly correlate with fluid salinity and therefore are not suitable as a "slab geothermometer". From a synopsis of experimental and melt inclusion data, it is suggested that the importance of sediment or slab melting in the generation of arc magmas is likely overestimated, while the effects of trace element scavenging from the mantle wedge may be underestimated. Moreover, establishing reliable datasets for the fluid/mineral partition coefficients of trace elements as a function of pressure, temperature and salinity requires additional efforts, since

most of the commonly used experimental strategies have severe drawbacks and potential pitfalls.

Keywords: Subduction zones, trace elements, halogens, chlorine, fluid flow, percolation, mantle wedge, slab geothermometer, arc magmas

INTRODUCTION

Together with mid-ocean ridges, subduction zones are the main sources of magma on Earth today and there is increasing evidence that this is so since billions of years (e.g. Tang et al. 2016). The continental crust is largely a product of calc-alkaline magmas produced in subduction zones. Accordingly, understanding magma generation in this environment is essential for any global picture of planetary evolution. Early studies suggested that calc-alkaline magmas may form by direct melting of the basaltic layer in the subducted slab (Green and Ringwood 1968). However, models of the thermal structure of subduction zones (Davies and Stevenson 1992, Rüpke et al. 2004, Syracuse et al. 2010) imply that at present geothermal gradients, the temperatures required for melting the basaltic layer may only be reached under unusual circumstances. Therefore, the "standard model" of magma generation in subduction zones (Gill 1981, Arculus and Powell 1986, Tatsumi 1989, Peacock 1990) assumes that aqueous fluids are released from the subducted slab during the breakdown of hydrous minerals such as amphibole. These fluids migrate upwards and trigger melting in the mantle wedge above the slab. Trace element abundances in calc-alkaline magmas likely reflect to some degree the chemical mobility in aqueous fluids. In particular, the "negative Nb-Ta anomaly", i.e. the strong depletion of Nb and Ta relative to many other incompatible elements, is believed to be due to the poor solubility of Nb and Ta in aqueous fluids. On the other hand, "fluid mobile elements", such as Rb or Ba are often strongly enriched in calc-alkaline magmas due to selective transport from the subducted slab to the mantle wedge by aqueous fluids. The detection of cosmogenic ^{10}Be in subduction zone magmas (Brown et al. 1982) provides direct evidence for the transport of material that one resided on Earth´s

surface into the zone of melting above the slab. Already Armstrong (1971) noted a close correlation between the $^{206}Pb/^{204}Pb$ ratio of arc magmas and the sediments in front of some arcs.

Research in the last decades has very much improved our understanding of subduction zone processes. Experimental studies demonstrated that amphibole dehydration is not the only source of aqueous fluids; rather there are numerous hydrous phases in the basaltic (MORB) layer and the sediments, including lawsonite and phengite, that may provide a source of water beyond the depth of amphibole dehydration (Schmidt and Poli 1998). Serpentine could be a very important source of water in the peridotitic part of the slab (Ulmer and Trommsdorf 1995; Rüpke et al. 2004), provided that deep fracturing allows some hydration by contact with seawater to occur. The direct observation of complete miscibility between silicate melts and water (Shen and Keppler 1997, Bureau and Keppler 1999) showed that under some circumstances, there may be a continuum of fluid compositions ranging from dilute aqueous fluids to hydrous silicate melts. Systematic studies of undegassed melt inclusions (Métrich and Wallace 2008 and references therein) constrained the typical water contents of primitive arc basalts to be between 2 and 6 wt. %, consistent with the model of fluid-triggered melting in the mantle wedge. An increasing oxidation state of the mantle wedge appears to be directly correlated with fluid addition (Kelley and Cottrell 2009). The fluid release from the subducted slab can in some cases be imaged by the inversion of magnetotelluric data (McGary et al. 2014). Radioactive disequilibria between ^{238}U, ^{230}Th, and ^{226}Ra constrain the timescale of fluid transfer from the subducted slab to the zone of melting to be typically in the range of 30 000 to 120 000 years, sometimes even shorter (e.g. Hawkesworth et al. 1997, Turner and Foden 2001).

Detailed studies of trace element abundances and ratios in various arcs have shown considerable variability. These variations may partially be due to differences in the composition of sediments and other materials entering the subduction zone (Plank and Langmuir 1993), partially they may reflect variations in the nature and transport capability of the fluids involved. In particular, Th and Ba often show a strikingly different behavior (e.g.

Hawkesworth et al. 1997, Woodhead et al. 2001; Pearce et al. 2005), with high Ba/Th ratios often being associated with a “shallow fluid component” while elevated Th contents may indicate a “deep subduction component”. For elements that are not highly mobile in fluids, different degrees of partial melting can account for a large part of the observed trace element variability (Turner and Langmuir 2015). Inferred degrees of melting appear to correlate with crustal thickness, implying that they are controlled by the thermal structure of the mantle wedge.

Any quantitative modeling of the transport processes in subduction zones requires experimental data on the fluid/mineral partitioning of trace elements. While numerous studies have reported such data (Brenan 1994, 1995, Keppler 1996, Stalder et al. 1998, Kessel et al. 2005, Bali et al. 2011, 2012), there are still considerable uncertainties and apparent contradictions among the data sets. Moreover, several studies suggested that some features in the composition of arc magmas, such as high Th/Ba and Th/U ratios, cannot be explained by fluid transport of trace elements and have instead invoked sediment melts as the main carrier of volatiles and trace elements from the slab to the mantle wedge (e.g. Kelemen et al. 2005, Hermann et al. 2006, Spandler and Pirard 2013). Such models appear to be consistent with slab surface temperatures high enough to intersect the water-saturated solidus of sediments (Syracuse et al. 2010) and with geochemical data that appear to imply similarly high temperatures (Plank et al. 2009). Unfortunately, the limitations and uncertainties in the experimental data on fluid/mineral partitioning, which provide essential constraints on possible models of magma generation in subduction zones, are often not well appreciated by non-specialists. Therefore, I provide here an overview over the basic properties of subduction zone fluids, the experimental methods for determining fluid/mineral partition coefficients, and the potential uncertainties in the available data. Finally, I will argue that the chemical composition of undegassed melt inclusions supports a dominant role of aqueous fluids as the main agent of chemical transport from the subducted slab into the mantle wedge.

SOME BASIC PROPERTIES OF SUBDUCTION ZONE FLUIDS

Figure 1 shows some properties of pure water as a function of pressure and temperature. Superimposed on these diagrams are two geotherms for the slab surface (Rüpke et al. 2004), for 80 million years old oceanic crust and subduction rates of 2 and 10 cm/year, respectively. Temperatures in the interior of the slab, 8 km below the surface (i.e. in the peridotitic part) are also shown. Since the slab is heated by conduction from the mantle wedge, the temperatures in the slab interior are much lower than on the surface. Depending on the parameters and model assumptions chosen, there can be a larger variation in slab geotherms (Syracuse et al. 2010); however, the geotherms shown in Figure 1 are still quite typical for most situations.

Density (Fig. 1 a) is the most important property of water. The density difference to the surrounding rock is the driving force for the ascent of fluids. More importantly, the solvent properties of a fluid are often much better described in terms of density and temperature, rather than pressure and temperature (e.g. Dolejs and Manning 2010; Bernini et al. 2013 a). As can be seen from Figure 1 a, the density of water along most of the subduction path falls into a rather narrow density range between 1.2 and 1.3 g/cm^3. Changes in solvent properties are therefore expected to be mostly a function of temperature.

The dielelectric constant (Fig. 1 b) of a solvent describes its ability to shield electrical charges and therefore, to dissolve solutes in ionic form. In a solvent containing polar molecules, such as H_2O, the dipoles align themselves around any ion such that they shield the electrical field (Weingärtner and Franck 2005). This effect facilitates charge separation and therefore dissolution in the fluid. The dielectric constant generally increases with pressure and with density, because of the increasing number of dipoles per volume. It decreases with temperature, because thermal motion counteracts the formation of an oriented dipole layer. Water at ambient condition has an exceptionally high dielectric constant near 80, which is responsible for its excellent solvent properties (Heger et al. 1980). Along most of the P,T path of the slab surface, the dielectric constant of water is reduced to a value around 30 - 40,

comparable to methanol or glycerol at ambient conditions (Sverjensky et al 2014). Accordingly, the capability of water to dissolve ionic species should be reduced.

Some phase boundaries are superimposed on the subduction geotherms in Figure 1c. Amphibole dehydration may release aqueous fluid at a depth around 70 km; serpentine may carry water to much greater depth with a possible release between 150 and 200 km. There are however, many dehydration reactions (not shown in Figure 1c) that may occur between amphibole and serpentine dehydration (Schmidt and Poli 1998). The two geotherms shown do not intersect the water-saturated solidus curves for sediment or MORB; however, more recent models suggest that for some slabs, such an intersection may occur (Syracuse et al. 2010). This does not, however, necessarily imply the formation of slab melts, because neither the sediments nor the meta-basalts will be water-saturated at this depth; they will have lost most of their water already due to dehydration reactions at much more shallow depth (< 100 km), so that their water content is likely reduced to values near 1 wt. % at most (Hacker et al 2008). In this situation, the water-saturated solidus does not determine the onset of melting; rather the beginning of melting is controlled by the dehydration solidus, where hydrous minerals (e.g. phengite) decompose to a hydrous silicate melt. Schmidt et al. (2004) showed that the fluid-absent solidus of sediment due to phengite breakdown is located at temperatures 200 – 300 ˚C above the water-saturated solidus. Such temperatures likely will only be reached under very unusual circumstances. Accordingly, melting of the slab or the sediment layer is not expected to be a very common phenomenon, except perhaps if aqueous fluid from the deep dehydration of serpentine is added to the sediment in an amount that is so high that it cannot be accommodated in hydrous minerals anymore.

Subduction zone fluids will never be pure water. They will contain a dissolved silicate component due to their interaction with the surrounding rock. If equilibrium is achieved with the rocks of the MORB / eclogite layer of the slab or with the peridotite in the mantle wedge, the resulting fluids will usually be rather dilute, containing only a few wt. % of dissolved silicate (Manning 2004, Sverjensky et al. 2014). The situation may be different, however, for fluids in equilibrium with the sediment layer that is more enriched in silica, alkalis, and

aluminum. The critical curve in the system albite-H_2O is located at rather low pressures and temperatures, e.g. near 600 ˚C at 2 GPa (Shen and Keppler 1997). This means that as the P, T conditions approach this critical curve, the solubility of albite component in water has to increase dramatically, such that very silica-rich fluids may be produced and ultimately, beyond the critical curve, complete miscibility exists between albite melt and water. Very silica-rich, "supercritical" fluids may therefore be generated inside the sediment layer already some 100 ˚C below the solidus by dehydration reactions along a hot geotherm, while they are out of equilibrium with either a peridotite or MORB lithology. Whether such fluids ultimately reach equilibrium with the mantle wedge during their upward percolation is a question that will be further discussed below. An interesting observation is, however, that these fluids will maintain a very low viscosity and high mobility up to rather high silicate contents (Fig. 2). Equilibrium with the surrounding rock will in general also control the pH of subduction zone fluids through reactions such as CaO (mineral) + H_2O (fluid) = Ca^{2+} (fluid) + 2 OH^- (fluid). Of the main constituent oxides of MORB and peridotite, SiO_2 is a very weak acid, Al_2O_3 is amphoteric, while MgO, CaO, Na_2O, and K_2O are moderately strong to strong bases. Accordingly, one would expect that fluids should be buffered to a slightly alkaline pH.

The reduced dielectric constant of water under subduction zone conditions implies that the ability of the fluid to dissolve ionic species is also reduced. Accordingly, ion pairs, polymeric species and neutral complexes are likely to be stabilized in such fluids. The availability of suitable complexing agents may therefore be an important factor in determining the ability of fluids to transport trace elements. Among the possible complexing agents, chloride is likely the most important one, due to its elevated abundance and chemical affinity. Figure 3 shows the concentration of Cl and of H_2O in undegassed olivine-hosted melt inclusions from arc basalts (Métrich and Wallace 2008). The absolute abundances of both Cl and H_2O are orders of magnitude higher than in MORB glasses (e.g. Saal et al. 2002) and accordingly, it is plausible that both H_2O and Cl were added to the magma source in the form of hydrous fluids. Black lines in Figure 3 show the salinity (in wt. % NaCl) of fluids that would be required to produce the observed Cl/H_2O ratios. It is obvious from this diagram that Cl-poor fluids, with less than 1 wt. % NaCl basically do not exist in subduction zones, while fluids with between 5

and 10 wt. % NaCl are quite common. The inferred salinities are quite consistent with fluid inclusion data from high-pressure metamorphic rocks and mantle xenoliths from subduction zones (Kawamoto et al. 2013, Kumagai et al. 2014, Frezzotti and Ferrando 2015), and with the composition of Cl-rich fluid inclusions in diamond that are interpreted as remnants of subduction zone fluids (Weiss et al. 2015). Interestingly, such Cl-rich inclusions of mantle fluids in diamond often contain exorbitantly high concentrations of incompatible trace elements, such as several wt. % of Sr and Ba (e.g. Klein Ben-David et al., 2007). Some salinity of subduction zone fluids is also required to account for the elevated electrical conductivity above dehydrating slabs inferred from magnetotelluric data (McGary et al. 2014), since pure water is a rather poor electrical conductor. Chloride is a moderately hard base and it should therefore form stable complexes with moderately hard acids, such as Rb^{+}, Ba^{2+}, Sr^{2+}, and Pb^{2+}, but not with very hard acids, like Nb^{5+} and Ta^{5+}. Complexing by chloride in aqueous fluid may therefore be very important for producing or enhancing the typical trace element signature seen in arc magmas (Keppler 1996). Moreover, the presence of chloride also affects the concentration of dissolved silica in a fluid. Cruz and Manning (2015) showed that the solubility of quartz in water is markedly reduced by the presence of NaCl. Together with variations in temperature, this effect could potentially produce two different suites of aqueous fluids in subduction zones, namely chloride-rich and silica-poor fluids on one hand, and chloride-poor, silica-rich fluids on the other hand.

EXPERIMENTAL METHODS FOR MEASURING FLUID/MINERAL PARTITION COEFFICIENTS

Why is it difficult to measure fluid/mineral partition coefficients?

To obtain the equilibrium distribution of a trace element between a fluid phase and a mineral, the trace element has to diffuse through the crystal lattice of the mineral. At temperatures of 400 to 1000°C, most relevant for the dehydration of the subducted slab, the diffusion coefficients of most trace elements in silicates are so low, that equilibrium cannot be achieved in experiments with reasonable run durations. To illustrate this, consider the diffusion of Ce in

clinopyroxene. According to van Orman et al. (2001) D_{Ce}= 7.94 · 10^{-5} m^2s^{-1} exp(- 463 $kJmol^{-1}$/RT). At 1000 ˚C, this yields a diffusion coefficient of 7.80 · 10^{-24} m^2s^{-1}, which translates into a mean diffusion path (according to $\bar{x}^2 = 2Dt$) of just 2.6 nm after 5 days. In other words, only the few outermost layers of atoms may be in equilibrium with the fluid after an experiment with reasonable run duration. At 600 ˚C, the estimated diffusion path is 1.15 · 10^{-4} nm, i.e. equilibrium cannot even be reached for the outermost atoms of the crystal.

The same problem is in principle also encountered in measuring mineral/melt partition coefficients. But for mineral/melt partition coefficients, there is an easy solution to this problem: By cooling a silicate melt, one can crystallize the mineral of interest out of the melt. If regimes of rapid growth due to strong supersaturation are avoided by slowly cooling the charge, one can assume that during its formation, any part of the crystal was in equilibrium with the melt. For a strongly incompatible element, the melt will act as an infinite reservoir and the concentration in the melt can often be easily determined by analyzing the glass phase after quenching the charge. If partition coefficients are strongly temperature-dependent, care has to be taken only to analyze the outermost rim of the crystal that was in contact with the final melt composition. This experimental strategy has yielded a wealth of very precise mineral/melt partition coefficients, which are also well understood from a theoretical point of view (e.g. Blundy and Wood 2003 and references therein). For fluid/mineral partitioning, however, the situation is very different. Crystallizing the mineral out of the fluid is usually not feasible, since the solubility of most silicate minerals in aqueous fluids is too low. Only under some favorable circumstances, recrystallization of minerals by dissolution and re-precipitation may occur, which allows equilibration with the fluid. Moreover, analyzing the fluid is not easy, because even during very fast quenching, the composition of the fluid often changes due to precipitation of solid phases. Accordingly, both attainment of equilibrium and accurate analysis of fluid composition are major challenges in this type of experiment. Various techniques have been proposed to overcome these problems, but nearly all of them have some limitations or potential pitfalls. It is for these reasons that data on fluid/mineral partitioning are subject to much larger uncertainty than mineral/melt partition coefficients.

Fluid/mineral from fluid/melt partition coefficients

If a silicate melt is in equilibrium with a mineral, and the same melt is in equilibrium with a fluid, then the mineral is also in equilibrium with the fluid. In such a situation, the Nernst partition coefficients for any element between these three phases are related to each other:

$$D^{fluid/mineral} = D^{fluid/melt} / D^{mineral/melt}$$

where $D^{fluid/mineral} = c_{fluid}/c_{mineral}$, $D^{fluid/melt} = c_{fluid}/c_{melt}$, and $D^{mineral/melt} = c_{mineral}/c_{melt}$. Keppler (1996) used this relationship to estimate fluid/mineral partition coefficients from measurements of fluid/melt partition coefficients and literature data on mineral/melt partition coefficients. $D^{fluid/melt}$ is relatively easy to measure, since diffusion coefficients in both the fluid and the melt phase are high, and therefore equilibrium is certainly reached within a few hours or days. A problem is still that during quenching of the fluid, part of the solute may precipitate. Keppler (1996) solved this problem by treating the run products with dilute HCl solution, assuming that this would re-dissolve any trace elements precipitated during quenching, while it should not significantly leach material out of the quenched glass. Indeed, in-situ X-ray fluorescence studies in diamond cells later showed that this method works well under appropriate circumstances (Borchert et al. 2010). However, the method has limitations and is difficult to directly apply to the P,T conditions deep in a subduction zone. With increasing P and T, the solubility of silicates in aqueous fluids increases greatly. Upon quenching from high pressure, these silicates may precipitate as melt droplets from the fluid. The resulting fine-grained beads of silicate glass are very difficult or impossible to distinguish from glass that formed by quenching the original melt phase. Therefore, this method works quite well at relatively low pressures, but is unsuitable for pressures above about 1 GPa. However, by using in-situ synchrotron X-ray fluorescence measurements in externally-heated diamond cells, measurements of fluid/melt partition coefficients above 1 GPa are possible (e.g. Borchert et al. 2010, Kawamoto et al. 2014).

Direct measurements of fluid/mineral partition coefficients

Despite the intrinsic difficulties in these experiments, several studies reported direct measurements of fluid/mineral partition coefficients. Brenan et al. (1995) used crystalline minerals (clinopyroxene and garnet) as starting material, together with a large excess of fluid. They observed some recrystallization of the minerals, i.e. the formation of new crystals or overgrowths, which were analyzed by ion probe after the experiment. Fluid compositions were not directly analyzed for trace elements; rather, it was assumed that the fluid formed a reservoir of constant composition during the experiment. The trace element concentrations in the fluid in equilibrium with the recrystallized minerals were therefore assumed to be the same as at the beginning of the experiment. Brenan et al. (1995) noted one potential source of error in this kind of experimental strategy: The solubilities of some of the high-field strength elements (HFSE) in aqueous fluids are so low that accessory oxide and silicate phases of Nb, Ta, U, or Th may precipitate at concentrations of a few ppm. If the fluid phase is not directly measured, partition coefficients then cannot be calculated anymore. If such an effect remains undetected, very large errors in partition coefficients may result. Brenan et al. (1995) solved this problem by reducing the initial concentration of these elements in the fluid below the level where accessory phases appeared to precipitate (< 10 ppm Nb + Ta, < 5 ppm U or Th, at 2 GPa and 900 ˚C).

In order to directly measure the fluid composition in fluid/mineral partitioning experiments, several studies (e.g. Stalder et al. 1998, Kessel et al. 2005) have used the diamond trap technology originally proposed by Ryabchikov et al. (1989). Here, the sample capsule contains the starting material together with a layer of diamond powder. The diamond powder provides some empty pore space, into which the fluid infiltrates during the experiment. Material that precipitates upon quenching of the experiment will be contained inside the diamond trap and can therefore be analyzed separately from the solid phases. Kessel et al. (2005) improved the conventional diamond trap method by introducing a cooling device that allows freezing of the entire aqueous solution contained in the diamond trap. This has the advantage that absolute concentrations of trace elements can be measured, e.g. by laser ablation. Otherwise, if only the solid residue after opening and drying the capsule is

328 measured, only relative concentrations of solutes can be obtained and absolute
329 concentrations need to be recalculated by mass balance.
330
331 Studies that use the diamond trap method usually make the implicit assumption that
332 everything that is found inside the diamond trap was originally dissolved in the fluid in
333 equilibrium with the solid mineral phases. However, this will not always be a valid assumption.
334 Figure 4 illustrates a potential problem in this kind of experiment. If a glass is used as starting
335 material – like in most studies using the diamond trap method – initially a super-saturated
336 solution will form, since glass is a metastable phase with high Gibbs free energy that
337 translates into an elevated solubility in water. This super-saturated solution will attain
338 equilibrium by precipitating some crystalline phases that will persist during the entire duration
339 of the experiment. This effect can be directly seen in the diamond anvil cell experiment shown
340 in Figure 4: Upon heating of a piece of andesite glass in water, first a super-saturated solution
341 forms that later precipitates some (not identified) mineral everywhere in the sample chamber.
342 In a diamond trap experiment, such precipitation will also occur within the diamond layer and
343 the material contained within will later be misidentified as a fluid component. Due to the very
344 low equilibrium solubility of many high-field strength elements in aqueous fluids, this can be a
345 very severe problem for these trace elements. For large-ion lithophile elements (LILE) that
346 are usually quite soluble in fluids, fewer problems are to be expected. The formation of a
347 super-saturated solution could of course be avoided, if experiments are started with the
348 mineral assemblage stable under run conditions. But in this situation, attainment of
349 equilibrium would again require the diffusion of trace elements through a crystal lattice, which
350 is not feasible within realistic run durations, as discussed above. In order to reach equilibrium
351 in a fluid – solid system, the solid has to precipitate from the fluid and this is most easily
352 achieved by using a metastable starting material, such as a glass (Kessel et al. 2005).
353 Accordingly, problems due to initial supersaturation of the fluid phase are likely unavoidable in
354 this kind of experiment. The magnitude of the problem may depend on the details of the
355 experimental protocol. For example, very slow heating rates may be helpful in avoiding strong
356 supersaturation. The effect of such parameters on the results of diamond trap experiments
357 has, however, never been systematically investigated.

Fluid/mineral partition coefficients from solubility measurements

Some trace elements, in particular the HFSE, tend to form highly refractory accessory phases, such as zircon ($ZrSiO_4$). If it is possible to measure the solubility of Zr in solid phases in equilibrium with zircon in one set of experiments and to measure the solubility of zircon in fluid in another set of experiments at the same P,T conditions, the fluid/mineral partition coefficient of Zr can be calculated as the ratio of the solubility in the fluid relative to the solubility in the mineral. Obviously, this is a rather tedious approach to fluid/mineral partitioning, because every element of interest has to be studied separately and at least two different experiments are required to obtain one single partition coefficient. However, the method has the potential to produce very accurate data, since problems with the supersaturation of fluids can be avoided and true attainment of equilibrium can be experimentally demonstrated.

In order to determine the solubility of a trace element in a mineral in equilibrium with a saturating phase, e.g. zircon, one can crystallize the mineral from an oxide mixture, a gel or similar starting materials in the presence of excess zircon and a fluid phase. Crystallization of the mineral will occur through the fluid phase, by first dissolving the starting material in the fluid and then precipitating the stable mineral out of the fluid. However, the important point here is that the saturating mineral – zircon in this example – has to be present in its stable form already at the beginning of the experiment. Therefore, the fluid from which the new phase precipitates will from the beginning be saturated, but not oversaturated with zircon, because oversaturation cannot be produced by dissolving a thermodynamically stable phase. The Zr content in the run product minerals therefore should reflect the equilibrium Zr solubility in the mineral coexisting with zircon.

For measuring the solubility of a mineral in fluids, several methods have been developed that can yield highly accurate results, if properly used. One method is to carefully measure the weight loss of a clean, polished single crystal after leaching it with a fluid at high P and T in a

388 piston cylinder experiment (Manning 1994). Upon quenching of the run to room temperature,
389 some material that was originally dissolved in the fluid at high P and T will usually precipitate.
390 However, due to the very fast quench, which limits the possible diffusion path length, this
391 precipitation will mostly happen inside the fluid, not on the surface of the crystal. Therefore,
392 the weight loss of the crystal can give accurate fluid solubilities. A variant of this method uses
393 a double capsule, where the crystal is contained in a perforated inner capsule that is sealed
394 together with the fluid into an outer capsule (Anderson and Burnham 1965). During the
395 experiment, fluid flow and diffusion between the outer and inner capsule is possible and
396 should yield a homogeneous fluid composition in equilibrium with the crystal. During quench,
397 some material from the fluid in the outer capsule may precipitate, but if the inner capsule is
398 carefully removed afterwards, one can assume that everything that was found in the outer
399 capsule originally was dissolved in the fluid. These weight loss and double capsule
400 experiments have yielded a wealth of data on mineral solubilities in fluids, both for abundant
401 minerals such as quartz (e.g. Anderson and Burnham 1965, Manning 1994) and for
402 accessory phases (e.g. Tropper and Manning 2005, Tropper et al. 2011). However, these
403 methods require very careful experimental protocols and in particular, temperature gradients
404 along the capsule have to be minimized as much as possible. Temperature gradients
405 exceeding 10 ˚C/cm are common in piston cylinder experiments, if no special care is taken.
406 Since mineral solubilities generally increase with temperature, this will cause material to be
407 dissolved in the hot part of the sample and re-precipitated in the cold part. This may cause
408 major errors both in the weight-loss and the double capsule technique. An illustrative example
409 here involves rutile TiO_2. In early experiments using the weight-loss technique, Ayers and
410 Watson (1993) reported rutile solubilities in water up to 1.9 wt. % at 1 GPa and 1100 ˚C. In a
411 later study, again using the weight loss technique in a piston cylinder apparatus, Tropper and
412 Manning (2005) found a maximum rutile solubility in water of less than 400 ppm by weight at
413 1000 – 1100 ˚C and 1 – 2 GPa, about two orders of magnitude below the results of Ayers and
414 Watson (1993). The likely reason for this discrepancy is improved experimental methods,
415 leading to lower temperature gradients in the Tropper and Manning (2005) experiments, as
416 well as a more careful discrimination between crystals formed during quenching and crystals
417 formed by material transport during the run. In general, the performance of the weight loss or

418 double capsule technique for solubility measurements in the piston cylinder apparatus will
419 depend on the properties of the system to be studied. Experimental problems are to be
420 expected for systems with a strong temperature dependence of the mineral solubility in water
421 and a low supersaturation-threshold for the nucleation of new crystals. Rutile-H_2O apparently
422 is such a system, while quartz-H_2O appears to be much more easy to study.
423
424 In order to overcome the difficulty in distinguishing quench crystals from crystals that formed
425 due to material transport during a solubility experiment, in-situ methods using externally
426 heated diamond anvil cells have been developed (Audetat and Keppler 2005). The principle is
427 shown in Figure 5. A crystal, in this case rutile, of precisely known dimension is placed inside
428 the sample chamber of a diamond cell filled with some fluid (pure H_2O in Fig. 5). The cell is
429 heated very slowly until the crystal completely dissolves in the fluid. The solubility is then
430 given by the ratio of the initial weight of the crystal to the weight of the fluid in the sample
431 chamber. Since the charge can be observed optically during the entire experiment, any
432 reprecipitation of material inside the sample chamber can be easily detected and
433 distinguishing quench crystals from crystals present during the run is not a problem.
434 Moreover, this method allows demonstrating true attainment of equilibrium. This is also
435 shown in Figure 5. If one heats the cell to a temperature just before the complete
436 disappearance of the crystal and then cools the cell down, one can see that the crystal starts
437 to grow again. This demonstrates that the solution became oversaturated during cooling.
438 Close inspection of Figure 5 shows that the crystal does not reach its original size again; this
439 is because some material also precipitates on the gasket, which demonstrates equilibrium
440 throughout the sample chamber. This precipitation is not seen in Figure 5, because the
441 crystals are out of focus; however, a picture showing the precipitation on the gasket can be
442 found in Audetat and Keppler (2005). Rutile solubilities in water obtained by this method are
443 still lower than those reported by Tropper and Manning (2005). In-situ synchrotron X-ray
444 fluorescence can be an alternative method for measuring mineral solubilities in fluids using
445 externally heated diamond cells; this method, however, requires careful calibration and
446 achievable detection limits are not always low enough to quantify solubilities at the ppm level
447 (e.g. Manning et al. 2008; Wilke et al. 2012). Moreover, the X-ray absorption of the diamond

precludes the analysis of light elements by this method and controlling of oxygen fugacity in diamond cells is nearly impossible.

Another promising method for measuring the solubility of trace elements in aqueous fluids makes use of synthetic fluid inclusions. Figure 6 shows synthetic fluid inclusions in quartz that were used to measure the solubility of UO_2 in a NaCl-bearing aqueous fluid (Bali et al. 2011, 2012). Such inclusions can be produced if a quartz crystal containing fractures is placed in a sample capsule containing a fluid and the phase to be investigated, in this case uraninite (UO_2). At high P and T, uraninite dissolves in the fluid and the fluid infiltrates the cracks in the quartz. Due to dissolution and re-precipitation of quartz, the fluid will ultimately be trapped in closed fluid inclusions. Such inclusions often also form in overgrowths on crystals during the experiment. After the run, the content of the inclusion can be analyzed by laser-ablation ICP/MS. Compared to the in-situ measurements in a diamond cell, this method has the advantage that oxygen fugacity can be controlled by external buffers; in diamond cells, an accurate control of oxygen fugacity is nearly impossible. Compared to the diamond trap technique, many separate samples of the fluid are available, such that inhomogeneities due to the accidental trapping of solid phases that precipitated earlier during the run can easily be identified. The large inclusion in Figure 6 shows some dark crystals of UO_2; they can be found in similar relative abundance (relative to the size of the inclusion) in other inclusions from the same run, indicating that they only precipitated during quenching and the material was originally homogeneously dissolved in the fluid.

IS THERE A DIFFERENCE BETWEEN FLUID/MINERAL AND MELT/MINERAL PARTITIONING?

This is not a trivial question. While it is widely believed that aqueous fluids and silicate melts cause different patterns of element partitioning with minerals, there are recurrent reports on experimental studies in the literature, which seem to suggest little or no element fractionation between melt and aqueous fluid (e.g. Adam et al. 1997, Louvel et al. 2014). This would imply

478 that fluid/mineral and melt/mineral partition coefficients are essentially the same. Some of
479 these data are probably accurate and can be understood from the phase relationships in
480 water-silicate melt systems. Other results may be experimental artifacts.
481
482 In silica-rich systems, such as albite-H_2O or haplogranite-H_2O (Shen and Keppler 1997,
483 Bureau and Keppler 1999), the critical curve, which determines the conditions under which
484 water and silicate melt become completely miscible, is located at rather low pressures and
485 temperatures (e.g. near 600 ˚C at 2 GPa for albite-H_2O). At conditions that approach the
486 critical curve, the silicate melt will dissolve more water and the fluid will dissolve more silicate,
487 such that at the critical curve the composition of the two phases becomes identical. This
488 necessarily means that the fluid/melt partition coefficient of any element has to approach unity
489 if the P,T conditions approach the critical curve. This is probably the reason for the rather
490 small fractionation of Zr observed by Louvel et al. (2014) in the system haplogranite-H_2O
491 ($D_{Zrf}^{fluid/melt}$ = 0.19 – 0.38 at 0.7 – 1.5 GPa and 575 – 745 ˚C). At P, T conditions not far away
492 from the critical curve in this system (e.g. 2 GPa and 735 ˚C, Bureau and Keppler 1999), such
493 a behavior is expected. Due to the silicate-rich nature of the aqueous fluid, the solubility of Zr
494 in the fluid is enhanced, while the high water content in the melt may reduce zircon solubility,
495 so that the solubility contrast of Zr in the two phases is diminished. One cannot, however,
496 conclude from such experiments that the solubility of Zr in aqueous fluids and silicate melts is
497 similar under conditions where the composition and the solvent properties of the two phases
498 are vastly different. Zircon ($ZrSiO_4$) solubility in pure aqueous fluids is exceedingly low (about
499 3 ppm Zr at 2 GPa and 1000˚C in equilibrium with zircon and quartz; Bernini et al. 2013 a),
500 while the solubility in a granitic melt is near 1300 ppm Zr at 1000 ˚C and greatly increases for
501 more depolymerized melts (Watson and Harrison 1983). This means that the fluid/mineral
502 partition coefficient of Zr should be at least three orders of magnitude smaller than the
503 melt/mineral partition coefficient. Accordingly, Zr will not be mobilized by pure aqueous fluids,
504 while it will readily partition into basaltic melts.
505
506 Adam et al. (1997) reported the results from piston-cylinder experiments in the system
507 trondjemite-H_2O and basanite-H_2O at 2 GPa and 900 – 1100 ˚C, which again appeared to

suggest very little fractionation of a wide suite of trace elements between silicate melt and fluid. To some degree, these results, particularly in the trondjemite-H_2O system, may again reflect the proximity to critical conditions. However, as Adam et al. (1997) pointed out themselves, it is very difficult, if not impossible, to distinguish quenched melt from quenched solutes (glass beads precipitated from the aqueous fluid during quenching) in these experiments. This difficulty may also explain why only little fractionation between melt and fluid was observed.

A REVIEW OF FLUID/MINERAL PARTITION COEFFICIENTS RELEVANT FOR SUBDUCTION ZONES

High field strength elements (Nb, Ta, Zr, Hf, Ti)

The high field strength elements are typically strongly depleted in arc magmas with the "negative Nb-Ta anomaly" being a particularly characteristic feature. This depletion is usually attributed to the inability of aqueous fluids to transport these elements. It is unquestionable that the HFSE partition very strongly into rutile, both in equilibrium with silicate melts and with fluids (Brenan et al. 1994). However, the data on the fluid/mineral partitioning for silicates (Table 1) are rather contradictory; for Nb and Ta experimentally determined fluid/mineral partition coefficients vary by nearly four orders of magnitude, e.g. for $D_{Nb}^{fluid/mineral}$ from 0.056 to 200 (Table 1). While the data of Keppler (1996) at 0.3 GPa and of Kessel et al. (2005) at 4 GPa suggest that Nb and Ta partition into clinopyroxene in equilibrium with aqueous fluids, Brenan et al. (1995) and Stalder et al. (1998) report preferential partitioning into the fluid phase at 2 to 5.7 GPa. The latter observation would imply that the negative Nb-Ta anomaly could only be produced by the retention of Nb and Ta in residual rutile, while the data of Keppler (1996) and Kessel et al. (2005) are consistent with the notion that the poor solubility of Nb and Ta in aqueous fluids causes the low abundance of Nb and Ta in arc magmas.

Some of the differences in the experimental results on the partitioning of Nb and Ta can perhaps be attributed to the physical condition under which the experiments have been

538 conducted. In particular, Kessel et al. (2005) noted that as P and T increases and the
539 aqueous fluid coexisting with minerals becomes richer in dissolved silicate, the fluid/mineral
540 partition coefficient of the HFSE increases. This is entirely consistent with various studies of
541 the solubility of rutile and zircon, which show a strong increase of Ti and Zr solubility with bulk
542 silicate content in the fluid (Audetat and Keppler 2005, Antignano and Manning 2008, Hayden
543 and Manning 2011, Wilke et al. 2012, Bernini et al. 2013a). Moreover, Brenan et al. (1995)
544 noted a strong dependence of the fluid/cpx partition coefficient of Nb on the Al content of the
545 pyroxene, with high Al contents favoring retention of Nb in the crystal. The Al contents in the
546 clinopyroxenes of the Brenan et al. (1995) study were rather low and the clinopyroxenes in
547 the experiments by Stalder et al. (1998) were essentially Al-free, which could perhaps explain
548 some of the rather high apparent fluid/melt partition coefficients of Nb and other HFSE
549 observed in these studies. Indeed, Baier et al. (2008) showed that the solubility of Nb in
550 clinopyroxene in equilibrium with $CaNb_2O_6$ greatly increases with tetrahedral Al and may
551 reach values up to 4 wt. % Nb_2O_5. $CaNb_2O_6$ is the phase that forms in a simplified basaltic
552 system upon addition of excess Nb_2O_5. In a pyroxene, the incorporation of Nb^{5+} requires
553 some charge compensation, e.g. by coupled substitution of Al^{3+} for Si^{4+}. Accordingly, a strong
554 dependence of Nb solubility and partitioning on Al content is expected. However, the study of
555 Baier et al. (2008) also clearly shows that the solubility of Nb in an aqueous fluid (~100 ppm
556 at 1000 ˚C and 1.5 GPa in equilibrium with $CaNb_2O_6$ and diopside) is orders of magnitude
557 smaller than Nb solubility in aluminous clinopyroxene, implying a $D_{Nb}^{fluid/cpx} << 1$. It therefore
558 appears likely that some of the rather high fluid/mineral partition coefficients of Nb and other
559 HFSE reported in Table 1 may have been affected by experimental artifacts, such as the
560 undetected precipitation of Nb oxides that were not accounted for in mass balance
561 calculations or that may have contaminated diamond traps.
562
563 On aggregate, the available experimental evidence suggests that Nb, Ta, Zr, and Hf are
564 rather insoluble in aqueous fluids and partition preferentially into the solid phase, even in the
565 absence of rutile. Rutile enhances the retention of the HFSE in the solid, but is not essential
566 for causing the HFSE depletion in the aqueous fluid. For rather silicate-rich aqueous fluids
567 that may form at higher P and T, the solubility of the HFSE in the fluid is somewhat enhanced

and may allow a minor, limited redistribution of HFSE under some circumstances (Woodhead et al. 2001). The presence of chloride has no strong effect on the partitioning of these elements, although a limited enhancement of solubility and fluid/melt partitioning at high Cl concentrations has sometimes been observed (Audetat and Keppler 2005, Bernini et al. 2013a). This effect is likely not due to the direct stabilization of some Cl complexes; rather, it may result from the increased ionic strength of the solution.

More high field strength elements (U, Th, W, Mo)

U, Th, W, and Mo are also high-field strength elements, but their behavior differs in several aspects from the "conventional" HFSE Nb, Ta, Zr, Hf, and Ti discussed in the previous section. Notably, U, W, and Mo may occur in various oxidation states (+4, + 5, and + 6) and accordingly, their behavior is redox sensitive. Unlike for the "conventional" HFSE, there is very strong observational evidence for Th being a mobile element that is added to the source of melting in many subduction zones (e.g. Hawkesworth et al. 1997, Woodhead et al. 2001). The somewhat different behavior of Th is likely related to the ionic radius of Th^{4+} (1.19 Å), which is much larger than the radii of Ti^{4+} (0.88 Å), Zr^{4+} (0.98 Å), and Hf^{4+} (0.97 Å; all values for eight-fold coordination after Shannon 1976). Th^{4+} is therefore an ion that shows a transition in its behavior from typical HFSE to a large-ion lithophile element. This simple concept explains all experimental observations quite well. Inspection of Table 2 suggests that Th may be retained in silicates, particularly clinopyroxenes at P,T conditions where the fluid is rather poor in dissolved silicate. However, as pressure and temperature increase and the fluid becomes more silicate-rich, Th starts to partition increasingly in favor of the fluid. The data of Keppler (1996) show that this may already occur far below the critical curve in the silicate-water system. The effect of Cl on the behavior of Th is rather minor.

The behavior of U^{4+} is likely quite similar to that of Th^{4+}. However, uranium may also occur as U^{6+} under more oxidizing conditions; U^{6+} forms the very stable uranyl complex ion (UO_2^{2+}), which is known to be highly soluble in water, particularly in the presence of chloride. Accordingly, $D_U^{fluid/clinopyroxene}$ varies by more than two orders of magnitude as a function of

598 oxygen fugacity and fluid salinity, from 0.61 at Co-CoO buffer conditions and in pure H_2O to
599 81 at the Re-ReO_2 buffer and in a saline fluid with 15 wt. % $NaCl_{eq}$ (at 2.6 GPa and 800 ˚C,
600 Bali et al. 2011, 2012). The U/Th ratio in arc magmas is therefore likely a good indicator of the
601 nature of the fluid involved in trace element transport. High U/Th indicates saline and
602 oxidizing fluids, while low U/Th ratios are typical for transport by silica-rich fluids.
603
604 Both W and Mo are quite atypical HFSE elements as they both partition strongly into a fluid
605 phase in equilibrium with silicates (Table 2). They are, however, somewhat retained in rutile
606 (e.g. $D_W^{fluid/rutile}$ = 0.8 and $D_{Mo}^{fluid/rutile}$ = 0.04 at 2.6 GPa, 1000 ˚C, Ni-NiO buffer and pure water
607 as fluid, Bali et al. 2012). This unusual behavior is likely due to the high stability of hydroxyl-
608 complexes of these elements in aqueous fluids. While the partitioning of W is independent of
609 fluid salinity and only slightly affected by oxygen fugacity, $D_{Mo}^{fluid/mineral}$ increases significantly
610 both with fO_2 and salinity, in very good agreement with field observations (König et al 2008,
611 Kirchbaur and Münker 2015). The abundance of W in arc magmas is therefore a particularly
612 good indicator of the total amount of the fluid added to the source, while the systematics in
613 the W-Mo-U-Th system can be used to tightly constrain both redox state and fluid salinity.
614 Quantitative modeling of the W, Mo, U, and Th abundances in arc magmas (Bali et al. 2012)
615 yields fluid salinities that are quite consistent with the Cl/H_2O ratios from melt inclusions of
616 primitive arc basalts (Fig. 3) and other sources of evidence.
617
618
619 **Large-ion lithophile elements (Cs, Rb, Ba, Sr, Pb)**
620 The LILE are generally considered to be “fluid-mobile” elements and indeed, all experimental
621 studies (Table 2) agree that Cs, Rb, and Ba will always strongly partition into the fluid relative
622 to garnet and pyroxene. For Sr and Pb, this behavior is less pronounced and may depend on
623 the P,T conditions and the composition of the fluid. No dependence of redox conditions is
624 expected or has ever been observed for these elements. There is, however, strong evidence
625 that the fluid/mineral partition coefficients of the LILE may greatly increase with fluid salinity.
626 Such an effect was observed by Keppler (1996) for Sr, Ba, Rb, and Pb and was confirmed by
627 Kawamoto et al. (2014) for Rb, Sr, and Pb and by Borchert et al. (2010) for Ba. On the other

hand, Stalder et al. (1998) claimed that Cl has no significant effect on the fluid/mineral partitioning of these elements. However, their study included only two experiments with Cl-bearing fluids and there is only a single pair of experiments carried out under otherwise equal conditions, where only the HCl content of the fluid varied. If one compares their experiments Nr. 57 and 64, $D_{Ba}^{fluid/garnet}$ increased from 16 to 59 and $D_{Sr}^{fluid/garnet}$ increased from 13 to 31 upon addition of 1.5 M HCl; only $D_{Pb}^{fluid/garnet}$ appeared to decrease.

Rare earth elements (REE)

With decreasing ionic radius, the heavy REE become less incompatible in minerals than the light REE and in garnet, the heavy REE usually behave as rather compatible elements. The data on fluid/mineral partitioning of the REE (Table 4) reflect this general trend. In equilibrium with a pure aqueous fluid, the light REE tend to partition slightly in favor of the clinopyroxene; the heavy REE are strongly retained in garnet. However, for more silica-rich fluids, the light REE appear to partition significantly into the fluid. Keppler (1996) already observed some enhancement of $D_{La}^{fluid/cpx}$ upon addition of Cl, but this effect could not be fully quantified. However, Tsay et al. observed that the solubility of $La_2Si_2O_7$ in water at 2.6 GPa increased 23-fold at 600 ˚C and 6-fold at 800 ˚C upon addition of just 1.5 m NaCl (5.5 wt. %). Similar, but somewhat smaller enhancements were also observed for the heavier REE. Tropper et al. (2011) reported an increase of $CePO_4$ solubility in water at 1 GPa and 800 ˚C by more than two orders of magnitude upon addition of up to 50 mol % NaCl. These data suggest that the fluid/mineral partition coefficients of the light REE should increase by at least an order of magnitude for the salinities expected for subduction zone fluids (Fig. 3), such that the light REE will become fluid-mobile in the presence of chloride.

A note on fluid/mineral partitioning in sediments

In some subduction zones, a significant fraction of the trace elements added to the zone of melting may ultimately be derived from subducted sediments (e.g. Plank and Langmuir 1993). Accordingly, some studies have looked at the fluid/mineral partitioning of trace elements in

subducted sediments (Johnson and Plank 1999, Melzer and Wunder 2000, Spandler et al. 2007). Unfortunately, the lithology of sediments in high-pressure metamorphic conditions is very complex, with numerous accessory phases, such as rutile, zircon, monazite, or phengite affecting and sometimes controlling the behavior of trace elements. Because of this complexity, a general assessment of the behavior of trace elements during the dehydration of sediments is difficult. Both Johnson and Plank (1999) and Melzer and Wunder (2000) observed for example a significant retention of Rb in phengite. This implies that at the depth where phengite becomes unstable, the composition of the fluid released should change markedly. There is, however, no clear evidence for such abrupt changes in fluid composition across subduction zones that could be unambiguously assigned to the destabilization of certain phases. This may perhaps imply that even in arcs where the sediment contribution to trace element flux may be significant, the fluids are often mixtures with components from different lithologies.

THE MESSAGE FROM UNDEGASSED MELT INCLUSIONS

Undegassed melt inclusions are the best source of information on the relationship between volatiles and trace elements in subduction zone magmas. Several studies have found relationships between water contents and “fluid mobile” trace elements such as Rb, Ba, or light REE in studies of melt inclusions or rapidly quenched submarine glasses (e.g. Stolper and Newman 1994, Cervantes and Wallace 2003). As noted above, there is now a large body of experimental evidence, which suggests that the capability of aqueous fluids to transport elements such as alkalis, alkaline earths, REE, and U is strongly enhanced by the presence of chlorine. Therefore, it should be possible to see such an effect as well in the melt inclusion data. In this context, the study of Cervantes and Wallace (2003) on undegassed melt inclusions in high-Mg basalts from various volcanoes in central Mexico is particularly interesting, since these samples span a wide range of Cl contents, from 0.08 to 0.196 wt. %. Therefore, if Cl indeed enhances trace element transport by fluids, the effect should be visible in this data set. For a “fluid mobile element”, such as Ce, a light rare earth, the ratio Ce/H_2O

688 should represent the Ce content in the fluid added to the source of melting, while the ratio
689 Cl/H_2O should give fluid salinity. Figure 7 shows a plot of Ce/H_2O versus Cl/H_2O for the data
690 set of Cervantes and Wallace (2003). There is a striking linear correlation between these two
691 parameters, with only one data point clearly falling off this trend. This abnormal data point
692 may be explained by post-entrapment water-loss from the inclusion. Such an effect would
693 move a point in this diagram on a straight line away from the origin. If one extrapolates this
694 line back to the trend delineated by the other inclusions, an initial water content for the
695 "abnormal" inclusion of 8.3 wt. % would be predicted. This value is high, but not implausible
696 for primary subduction zone magmas. Note that the trend in Figure 7 can neither be a result
697 of partial melting or fractional crystallization nor of degassing nor of post-entrapment water
698 loss. The Ce/H_2O ratio is known to be unfractionated by partial melting and fractional
699 crystallization in MORB and OIB (e.g. Michael 1995) and the high Mg content of the samples
700 makes it likely that they are primary magmas. Degassing would decouple a volatile element
701 like Cl from a non-volatile elements like Ce. Moreover, the high CO_2 contents of these
702 inclusions rule out any significant degassing. Post-entrapment water loss could produce a
703 linear array of data in this diagram; however, such an array would have to pass through the
704 origin of the plot, as water-loss leaves the Ce/Cl ratio unchanged. In reality, the Ce/Cl weight
705 ratio in these samples varies widely, from 0.023 to 0.085. The linear trend cannot be
706 produced by the mixing of two endmembers either, because water contents vary randomly
707 along the line. Therefore, the only plausible explanation for the trend seen in Figure 7 is that
708 Cl does indeed strongly enhance the transport of Ce by subduction zone fluids.
709
710 Figure 8 shows that not only Ce, but also Rb, Sr, La, and U normalized to H_2O show strong
711 positive correlation with Cl/H_2O in the melt inclusion data set from Mexico. The study of
712 Portnyagin et al. (2007) provides an even larger data set of undegassed melt inclusions in
713 olivine from arc basalts of several volcanoes in Kamchatka. Again, there are clear positive
714 correlations of Sr/H_2O, La/H_2O, Ce/H_2O, and U/H_2O with Cl/H_2O (Fig. 9). The relatively large
715 scatter in the data for U may reflect variations in redox state in the fluid source, as the fluid
716 solubility and fluid/mineral partitioning of U is known to be very redox sensitive (Bali et al.
717 2011, 2012). The Yb/H_2O and Nb/H_2O ratio in Kamchatka basalts is not affected by Cl/H2O,

except perhaps at very high fluid salinities. This would be consistent with Yb and Nb not being fluid mobile, except perhaps at high salinities, again in good agreement with experimental data. The behavior of Th (not shown) is qualitatively similar to Nb. Again, it is important to stress that the correlations seen in Figure 7 - 9 cannot be produced by variations in crystal fractionation or the degree of melting. Sr and Yb, for example, are more compatible than H_2O, while Cl is more incompatible (Dalou et al. 2012, Bernini et al. 2013b). Accordingly, fractional crystallization or partial melting should produce some inverse correlation between Sr/H_2O or Yb/H_2O and Cl/H_2O, the opposite of what is observed in Figure 8 and 9. Ce/H_2O should not be fractionated by such processes at all.

The fact that both data from Mexico and Kamchatka show qualitatively similar correlations of some incompatible elements with Cl/H_2O suggests that this is likely a global phenomenon, since these two subduction zones differ in many parameters, notably sediment input, which is large for Mexico, but small or absent for Kamchatka. Indeed, other data sets show similar effects as well; strong positive correlations between Ce/H_2O and Cl/H_2O can for example also be observed for a suite of olivine-hosted melt inclusions in high-Mg andesites from the Mount Shasta region in California (Ruscitto et al. 2011) or for submarine glasses from the Lau backarc basin that were likely affected by a subduction fluid (Peate et a. 2001, Kent et al. 2002). Differences in incompatible element/H_2O ratios at the same Cl/H_2O may be related to differences in the P,T conditions of fluid transport and/or to the nature and trace element content of the subducted material. The much higher Ce/H_2O ratios observed for Mexico (Fig. 7) as compared to Kamchatka (Fig. 9) may for example reflect the effect of a Ce-rich sediment component in the Mexican subduction zone.

From the foregoing discussion, it appears that plotting incompatible element/H_2O ratios versus the Cl/H_2O ratio from undegassed melt inclusions, as in Figures 7 – 9 is a useful tool for detecting trace element transport by dilute, Cl-bearing fluids in subduction zones. For a correct interpretation of these diagrams, however, the following points have to be considered:

(1) If a trace element already strongly partitions into the fluid in the absence of Cl, any further increase of fluid/mineral partitioning by Cl may be hard to detect. For example, for an incompatible element with a bulk fluid/mineral partition coefficient of 100, 5 % of fluid in a system would already extract 83 % of the total mass of this element. An increase of $D^{fluid/melt}$ to 1000 would increase this fraction to 98 %. This translates into an increase of the concentration of this element in the fluid by less than 20 % relative, which may be hard to detect, given the influence of other factors, such as variable P,T, and source composition across an arc. Accordingly, for extremely incompatible and fluid-mobile elements, such as Cs or Ba, Cl complexing, even if it occurs, may not always lead to strong correlations of Cs/H_2O or Ba/H_2O with Cl/H_2O. The effect of complexing is most clearly seen, if an element changes from a slightly compatible to an incompatible behavior upon addition of Cl. This is likely the case for La and Ce. Interestingly, the trend in Figure 7 does not extrapolate through the origin. This may imply that Ce remains compatible at low salinity, so that fluid transport does not significantly contribute to the Ce budget in the source of melting, and only above a Cl/H_2O ratio of about 0.02, Ce is effectively transported by the fluid. As noted above, such an effect may occur at even higher salinities for Yb and Nb (Fig. 9).

(2) Diagrams like Figures 7 – 9 are only meaningful for undegassed melt inclusions that suffered no significant post-entrapment loss of water. Since both the variables plotted on the x- and the y-axis have H_2O in the denominator, diffusional loss of water could produce a spurious linear trend passing through the origin of the diagram.

IMPLICATIONS

Is Ce/H_2O a slab geothermometer?

Experimental data suggest that the solubility of REE-bearing phases, such as monazite or allanite, in silicate melts and aqueous fluids strongly increase with temperature. Plank et al. (2009) suggested that the high Ce/H_2O ratios found in natural, undegassed melt inclusions may therefore reflect high temperatures at the slab surface. The highest temperatures, which

would be indicative of element transport by silicate melts, rather than aqueous fluids, were inferred from a set of melt inclusions from Mexico. This is exactly the set of data shown in Figure 7, where a clear correlation exists between Ce/H_2O and Cl/H_2O. Figure 9 shows a similar correlation for Kamchatka. Accordingly, it is likely that the primary parameter controlling Ce/H_2O is fluid salinity. This is consistent with experimental data by Tropper et al. (2011), who showed that the solubility of $CePO_4$ monazite in water at 1 GPa and 800 ˚C increases by a factor of 200 from pure water to an aqueous fluid with 50 mol % of NaCl. More recently, Tsay et al. (2014) showed that the solubility of $La_2Si_2O_7$ at 2.6 GPa and 800 ˚C increases by nearly an order of magnitude in 1.5 m NaCl solution (about 8 wt. % NaCl) compared to pure water. Note that such and even much higher salinities are common according to melt inclusion data (Fig. 3). Therefore, without an explicit correction for fluid salinity, it is unlikely that the Ce/H_2O ratio is a reliable measure of slab temperature. The high temperature inferred for some subduction zones (up to 901 ˚C for Mexico, Cooper et al. 2012) are likely vastly overestimated and as such, the data cannot be used to argue for extensive melting in the slab. Moreover, using Ce/H_2O as a geothermometer implies the assumption that this ratio is inherited from the slab and does not change upon percolation of the fluid through the mantle wedge. This will be further discussed below.

What causes magma generation in subduction zones?

Temperatures in subduction zones are lower than in the average mantle. Direct melting of the basaltic portion of the slab may only occur in very hot slabs. Therefore, the main mechanism for melting is likely melting point depression by the addition of water to the mantle wedge. However, whether water is transported from the slab to the mantle wedge as a rather dilute aqueous fluid or as a hydrous silicate melt, or a combination of them, is still being debated. The systematic correlations between incompatible trace element/H_2O ratios and Cl/H_2O in Figures 7 – 9 provide some new evidence on this subject. The correlations are consistent with trace element transport by dilute, chloride-bearing aqueous fluids. The enhancement of the solubility and fluid/melt partitioning of LILE elements (e.g. Rb, Sr; Keppler 1996), REE (Tropper et al. 2011, Tsay et al. 2014), and U (Bali et al. 2011, 2012) is well documented in

807 experimental studies. There is no experimental indication that Cl would have a similar effect
808 enhancing the solubility or melt/mineral partitioning of these elements in hydrous silicate
809 melts. Already the low solubility of Cl in silicate melts makes such an effect rather unlikely. Cl
810 solubility in silicate melts varies as a function of melt composition, pressure, and temperature,
811 but for the silica-rich melts expected to form from sediment melting, it is typically below 1 wt.
812 % (Webster et al. 2015). Ponader and Brown (1989) studied the speciation of La, Gd, and Yb
813 in Cl-containing silicate glasses and found no evidence for REE-Cl complexing. The possible
814 effect of small concentrations of Cl on the solubility of REE in silicate melts has not been
815 studied. But experimental studies have been carried out for fluorine, which is much more
816 soluble in silicate melts than chlorine. However, even for fluorine, no effect was observed on
817 the solubility of monazite or xenotime in silicate melts (Keppler 1993; Duc-Tin and Keppler
818 2015). Direct evidence for the absence of Cl-complexing in silicate melts comes from data on
819 the effect of Cl on the fluid/melt partition coefficient of trace elements. These studies show
820 that Cl strongly enhances the partitioning of alkalies, alkaline earths, REE and other elements
821 into the fluid, both at crustal and upper mantle P,T conditions (e.g. Keppler 1996, Borchert et
822 al. 2010, Kawamoto et al. 2014); if there were complexing by Cl in the melt in a similar extent
823 as it occurs in the fluid, the partition coefficient should be independent of Cl concentration.
824
825 The data in Figures 7 – 9 suggest that most of the LILE (e.g. Rb, Sr), light REE, and U were
826 transported to the zone of melting below Mexico and Kamchatka by chloride-containing
827 aqueous fluids. The observed trace element/water ratios suggest that the fluids contained up
828 to about 30 ppm of U, 5000 ppm Ce, 2000 ppm La, 1000 ppm Rb, and 4 wt. % Sr. These
829 numbers appear high, but they are in very good agreement with the trace element
830 concentrations sometimes observed in saline inclusions in diamonds, which may reach
831 several wt. % for Sr and Ba (e.g. Klein-BenDavid et al., 2007).
832
833 The effect of Cl on trace element partitioning eliminates several arguments against aqueous
834 fluids as the main agent of water and trace element transport from the slab to the mantle
835 wedge. As noted above, the observed high Ce/H_2O ratios are rather a product of high fluid
836 salinity than a result of high slab surface temperatures that may imply melting. Kelemen et al.

837 (2005) and others suggested that the light REE enrichments in arc magmas cannot be
838 produced by fluid transport, because of the low fluid/mineral partition coefficients for Ce and
839 La. This is, however, only so, if Cl-free aqueous fluids are considered. For a pure aqueous
840 fluid, the fluid/mineral partition coefficient of La and Ce for an eclogitic assemblage is indeed
841 between 0.1 and 1 (e.g. Kessel et al. 2005). However, the data by Tropper et al. (2011) and
842 Tsay et al. (2014) clearly show that the solubility of light REE in aqueous fluids may increase
843 by two orders of magnitude upon addition of Cl; accordingly, the fluid/mineral partition
844 coefficient of these elements may increase by a similar factor, depending on Cl concentration.
845 The effect of Cl complexing in the fluid may also explain why a correlation of the abundance
846 of fluid-mobile trace elements with water is not always observed. There is usually only a
847 limited range of primary water contents in undegassed melt inclusions; however, relatively
848 subtle variations in fluid salinity can cause major changes in the capability of these fluids to
849 dissolve trace elements. Stolper and Newman (1994) found a very good correlation between
850 trace element abundances and water contents for the Mariano trough magmas that were
851 likely affected by some subduction-related fluid content. Some positive correlation between
852 water contents and fluid-mobile trace elements was also observed by Cervantes and Wallace
853 (2003) in Mexico, while Portnyagin et al. (2007) did not observe such a correlation in
854 Kamchatka. Accordingly, they concluded that fluid transport cannot be responsible for the
855 trace element enrichment in the arc magmas of Kamchatka. However, Figure 9 shows their
856 data set and if trace element abundances are normalized to water and plotted against Cl/H_2O,
857 clear correlations are observed.
858
859 Melting of the sediment layer in the subducted slab may well occur under some
860 circumstances and such sediment melts may contribute to the transport of material from the
861 slab to the mantle wedge. However, slab surface temperatures that are comparable or higher
862 than the water-saturated solidus of sediments (Syracuse et al. 2010) do not necessarily imply
863 melting, because the sediments will not be water-saturated anymore at this depth (Hacker
864 2008; Schmidt et al. 2004). High Th contents and high Th/U ratios in arc magmas are not
865 conclusive evidence for the involvement of melts in trace element transport, as such features
866 can also be produced by silica-rich aqueous fluids (Table 2). On the other hand,

metasomatism by silicate melts cannot produce the short timescales inferred from radioactive disequilibria (Hawkesworth et al. 1997, Turner and Foden 2001), as models for the transport of such partial melts rather predict timescales of millions of years (Gerya and Yuen 2003). Moreover, if melts were the main carriers of volatiles to the mantle wedge, producing a typical primary arc basalt with 4 - 5 wt % water would require a massive addition of sediment melt to the source. This would not only alter the trace element budget, but also the stable phase assemblage, by stabilizing phlogopite and potentially exhausting olivine (Mallik et al. 2015). The melts produced in such a metasomatized mantle are not normal arc basalts anymore, but ultrapotassic magmas (Mallik et al. 2015). Such magmas are indeed observed in some volcanic arcs (e.g. Kirchbaur and Münker 2015) and they may indicate a major involvement of sediment melts in mantle metasomatism; they are, however, distinctly different from normal arc basalts or andesites.

Fluid flow and element scavenging in the mantle wedge

The idea that some of the trace elements entering the zone of melting in arcs are scavenged by aqueous fluids during their passage through the mantle wedge has been proposed a long time ago (Arculus and Powell 1986, Stolper and Newman 1994), but appears to have become less popular in recent years. Relatively non-radiogenic Sr isotopes in some arc magmas would be consistent with a mantle wedge origin of the Sr, rather than Sr coming from the subducted slab (Hawkesworth 1997). The high Cl/H_2O ratios observed in many arc basalts may also result from extensive fluid/rock interaction (Bernini et al. 2013b). Since Cl is more incompatible than water in mantle peridotite, fluid/rock interaction during passage through the mantle wedge will tend to selectively remove water from the fluid and therefore increase salinity. Bernini et al. (2013b) calculated the amount of peridotite required to increase the Cl/H_2O ratio to the values frequently found in melt inclusions of arc magmas (Fig. 3), starting from salinities close to seawater. While some of the observed Cl/H_2O ratios require little or no fluid/rock interaction, the most extreme values would imply equilibrated rock/fluid mass ratios near 3000. This would very likely also imply a significant contribution of trace element scavenging to the budget of fluid-mobile elements in arc magmas.

Radioactive disequilibria between ^{238}U and ^{230}Th constrain the timescale for fluid transfer from the slab to the source of melting to be in the range of 30 000 to 120 000 years (Hawkesworth et al. 1997), sometimes maybe as low as a few thousand years (Turner and Foden 2001). These rather short timescales could perhaps suggest that the flow of fluids through the mantle wedge is mostly channeled, with little interaction with the mantle peridotite and therefore little trace element scavenging. This is, however, not necessarily so. The diameter of fluid channels consistent with the observed timescales for fluid transfer can be roughly estimated from the Hagen-Poisseuille equation for laminar flow in a tube, which may be stated as

$$v = \frac{r^2}{8\eta}\left(\frac{dp}{dx}\right)$$

where v is the linear velocity, r is the radius of the tube, η is the viscosity, and (dp/dx) is the pressure gradient in flow direction. Assuming vertical tube-shaped channels, the pressure gradient is equivalent to the difference in hydrostatic pressure between the fluid column and the column of surrounding rock:

$$\left(\frac{dp}{dx}\right) = \Delta\rho g$$

where $\Delta\rho$ is the density difference between rock and fluid and g is the gravitational acceleration. For a vertical distance of 50 km between the slab surface and the zone of melting and a transfer time of 50 000 years, the fluid velocity is $3.3 \cdot 10^{-8}$ ms^{-1}. With $\Delta\rho$ of 2.5 g cm^{-3} and a fluid viscosity of 10^{-4} Pas (see Fig. 2), one obtains tube radius of just 32 nm, i.e. the diameter of the tube is only one order of magnitude larger than the typical width of grain boundaries. For a fluid viscosity of 10^{-2} Pas, a tube radius of 0.3 μm would be obtained. This is of course only a very approximate calculation and a realistic model of fluid transport would have to take other effects, such as the convective flow of the mantle wedge itself into account

925 (e.g. Wilson et al. 2014). However, the main result of this calculation, that the short
926 timescales of fluid transfer are still consistent with fluid flow through rather narrow channels,
927 is likely correct. The volume of rock that may equilibrate with the fluid during its passage
928 through the mantle wedge can be estimated from the magnitude of the free diffusion path
929 perpendicular to the flow direction for the same transfer time, i.e. 50 000 years. Using an
930 effective diffusion coefficient for water in polycrystalline olivine of $8.5 \cdot 10^{-10}$ m^2 s^{-1} at 1000 °C
931 (Demouchy 2010), one obtains a characteristic diffusion length in the order of 50 m. These
932 numbers show that even during the apparently short timescales of fluid transfer, equilibration
933 with a much larger volume of rock is certainly possible for water. For many trace elements,
934 diffusion coefficients are much lower. Using the data for Ce diffusion in clinopyroxene from
935 van Orman et al. (2001), one can estimate the free diffusion path of Ce to be about 5 μm over
936 50 000 years. This number is small, but still one to two orders of magnitude larger than the
937 estimated radius of the fluid channel, implying that requilibration of the fluid with a 10^2 – 10^4
938 times larger volume of rock is feasible under some circumstances. This is even more
939 plausible for univalent and divalent trace elements, such as Li, Sr, and Pb, where diffusion
940 coefficients in clinopyroxene and other silicates are orders of magnitude higher than for REE
941 (Cherniak and Dimanov 2010 and references therein). Accordingly, it appears plausible that
942 at least under some circumstances, scavenging from the mantle wedge may significantly
943 contribute to the flux of relatively mobile LILE elements to the zone of melting, in addition to
944 the slab component.
945
946 **CONCLUSIONS**
947
948 Both aqueous fluids and silicate melts may transport volatiles and trace elements from the
949 subducted slab to the zone of melting in volcanic arcs. From a review of experimental and
950 melt inclusion data, it is concluded that aqueous fluids are the dominant agents for chemical
951 transport and that the importance of silicate melts is often overestimated, while the
952 importance of element scavenging from the mantle wedge may be underestimated. Many
953 arguments that have been put forward against aqueous fluids as main transport medium
954 become invalid, once the strong enhancement of the transport capability of these fluids by

chloride is considered. For a fully quantitative modeling of subduction zone processes, additional experimental efforts are required to explore fluid/mineral partition coefficients over the entire relevant pressure, temperature, and salinity range. Such studies should also include serious efforts to benchmarks different experimental methods against each other.

ACKNOWLEDGEMENTS

Constructive reviews by Jim Webster, Alexandra Tsay and Adam Kent helped to improve this manuscript.

REFERENCES CITED

Adam, J., Green, T.H., Sie, S.H., and Ryan, C.G. (1997) Trace element partitioning between aqueous fluids, silicate melts and minerals. European Journal of Mineralogy, 9, 569-584.

Anderson, G.M., and Burnham, C.W. (1965) The solubility of quartz in supercritical water. American Journal of Science, 263, 494-511.

Antignano, A., and Manning, CE (2008) Rutile solubility in H_2O, H_2O-SiO_2, and H_2O-$NaAlSi_3O_8$ fluids at 0.7-2.0 GPa and 700-1000 ˚C: Implications for mobility of nominally insoluble elements. Chemical Geology, 255, 283-293.

Arculus, R.J., and Powell, R. (1986) Source component mixing in the regions of arc magma generation. Journal of Geophysical Research, 91, 5913-5926.

Armstrong, R.L. (1971) Isotopic and chemical constraints on models of magma genesis in volcanic arcs. Earth and Planetary Science Letters, 12, 37-142.

Audetat, A., and Keppler, H. (2004) Viscosity of fluids in subduction zones. Science, 303, 513-516.

983 Audetat, A., and Keppler, H. (2005) Solubility of rutile in subduction zone fluids, as
984 determined by experiments in the hydrothermal diamond anvil cell. Earth and Planetary
985 Science Letters, 232, 393-402.
986 Ayers, J.C., and Watson, E.B. (1993) Rutile solubility and mobility in supercritical aqueous
987 fluids. Contributions to Mineralogy and Petrology, 114, 321-330.
988 Baier, J., Audetat, A., and Keppler, H. (2008) The origin of the negative niobium tantalum
989 anomaly in subduction zone magmas. Earth and Planetary Science Letters, 267, 290-
990 300.
991 Bali, E., Audetat, A., and Keppler, H. (2011) The mobility of U and Th in subduction zone
992 fluids: an indicator of oxygen fugacity and fluid salinity. Contributions to Mineralogy and
993 Petrology, 161, 597-613.
994 Bali, E., Keppler, H., and Audetat, A. (2012) The mobility of W and Mo in subduction zone
995 fluids and the Mo-W-Th-U systematics of island arc magmas. Earth and Planetary
996 Science Letters, 351, 195-207.
997 Bernini, D., Audetat , A., Dolejs, D., and Keppler, H. (2013 a) Zircon solubility in aqueous
998 fluids at high temperatures and pressures. Geochimica et Cosmochimica Acta, 119,
999 178–187.
1000 Bernini, D., Wiedenbeck M., Dolejs, D., and Keppler, H. (2013 b) Partitioning of halogens
1001 between mantle minerals and aqueous fluids: implications for the fluid flow regime in
1002 subduction zones. Contributions to Mineralogy and Petrology, 165, 117-128.
1003 Blundy, J. and Wood, B. (2003) Partitioning of trace elements between crystals and melts.
1004 Earth and Planetary Science Letters, 210, 383-397.
1005 Borchert, M., Wilke, M., Schmidt, C., Cauzid, C., and Tucoulou, R. (2010) Partitioning of Ba,
1006 La, Yb and Y between haplogranitic melts and aqueous solutions: An experimental
1007 study. Chemical Geology, 276, 225–240.
1008 Brenan, J.M., Shaw, H.F., Phinney, D.L., and Ryerson, F.J. (1994) Rutile-aqueous fluid
1009 partitioning of Nb, Ta, Hf, Zr, U and Th: implications for high-field strength element
1010 depletions in island arc basalts. Earth and Planetary Science Letters, 128, 327-339.
1011 Brenan, J.M., Shaw, H.F., Ryerson, F.J., and Phinney, D.L. (1995) Mineral-aqueous fluid
1012 partitioning of trace elements at 900 ˚C and 2.0 GPa: Constraints on the trace element

chemistry of mantle and deep crustal fluids. Geochimica et Cosmochimica Acta, 59, 3331-3350.

Brown, L., Klein, J., Middleton, R., Sacks, I.S., and Tera, F. (1982) ^{10}Be in island-arc volcanoes and implications for subduction. Nature, 229, 718-720.

Bureau, H., and Keppler, H (1999) Complete miscibility between silicate melts and hydrous fluids in the upper mantle: experimental evidence and geochemical implications. Earth and Planetary Science Letters, 165, 187-196.

Cervantes, P., and Wallace, P.J. (2003) Role of H_2O in subduction-zone magmatism: New insights from melt inclusions in high-Mg basalts from central Mexico. Geology, 31, 235-238.

Cherniak, D.J., and Dimanov, A. (2010) Diffusion in pyroxene, mica and amphibole. Reviews in Mineralogy and Geochemistry, 72, 641-690.

Cooper, L.B., Ruscitto, D.M., Planck, T., Wallace, P.J., Syracuse, E.M., and Manning, C.E. (2012) Global variations in H_2O/Ce: 1. Slab surface temperatures beneath volcanic arcs. Geochemistry, Geophysics, Geosystems, 13, doi:10.1029/2011GC003902.

Cruz, M.F., and Manning, C.E. (2015) Experimental determination of quartz solubility and melting in the system SiO_2-H_2O-NaCl at 15-20 kbar and 900-1100 ˚C: implications for silica polymerization and the formation of supercritical fluids. Contributions to Mineralogy and Petrology, 170, Article Number: 35.

Dalou, C., Koga, K.T., Shimizu, N., Boulon, J., and Devidal, J.L. (2012) Experimental determination of F and Cl partitioning between lherzolite and basaltic melt. Contributions to Mineralogy and Petrology, 163, 591-609.

Davies, J.H., and Stevenson, D. J. (1992) Physical model of source region of subduction zone volcanics. Journal of Geophysical Research, 97, 2037-2070.

Demouchy, S. (2010) Diffusion of hydrogen in olivine grain boundaries and implications for the survival of water-rich zones in the Earth's mantle. Earth and Planetary Science Letters, 295, 305–313.

Dolejs, D., and Manning, C. E. (2010) Thermodynamic model for mineral solubility in aqueous fluids: theory, calibration, and application to model fluid-flow systems. Geofluids, 10, 20–40.

1043 Duc-Tin, Q., and Keppler, H. (2015) Monazite and xenotime solubility in granitic melts and the
1044 origin of the lanthanide tetrad effect. Contributions to Mineralogy and Petrology, 169,
1045 Article Number 8.
1046 Frezzotti, M.L., and Ferrando, S. (2015) The chemical behavior of fluids released during deep
1047 subduction based on fluid inclusions. American Mineralogist, 100, 352-377.
1048 Gerya, T.V., and Yuen, D.A. (2003) Rayleigh-Taylor instabilities from hydration and melting
1049 propel 'cold plumes' at subduction zones. Earth and Planetary Science Letters, 212,
1050 47-62.
1051 Gill J (1981) Orogenic Andesites and Plate Tectonics. Springer Berlin.
1052 Green, T.H., and Ringwood, T.E. (1968) Genesis of the calc-alkaline igneous rock suite.
1053 Contributions to Mineralogy and Petrology, 18, 105-162.
1054 Hacker, B.R. (2008) H_2O subduction beyond arcs. Geochemistry, Geophysics, Geosystems,
1055 9, Q03001, doi:10.1029/2007GC001707
1056 Hawkesworth, C.J., Turner, S.P., McDermott, F., Peate, D.W., and van Calsteren, P. (1997)
1057 U-Th isotopes in arc magmas: Implications for element transfer from the subducted
1058 crust. Science, 276, 551-555.
1059 Hayden, L.A., and Manning, C.E. (2011) Rutile solubility in supercritical $NaAlSi_3O_8$-H_2O fluids.
1060 Chemical Geology, 284, 74-81.
1061 Heger, K., Uematsu, M., and Franck, E. U. (1980) The static dielectric constant of water at
1062 high pressures and temperatures to 500 MPa and 550 °C. Berichte der
1063 Bunsengesellschaft für Physikalische Chemie, 84, 758-762.
1064 Hermann, J., Spandler, C., Hack, A., and Korsakov, A.V. (2006) Aqueous fluids and hydrous
1065 melts in high-pressure and ultra-high pressure rocks: Implications for element transfer
1066 in subduction zones. Lithos, 92, 399-417.
1067 Johnson, M.C., and Plank, T. (1999) Dehydration and melting experiments constrain the fate
1068 of subducted sediments. Geochemistry, Geophysics, Geosystems, 1,
1069 doi:10.1029/1999GC000014.
1070 Kawamoto, T., Mibe, K., Bureau, H., Reguer, S., Mocuta, C., Kubsky, S., Thiaudiere, D., Ono,
1071 S., and Kogiso, T (2014) Large-ion lithophile elements delivered by saline fluids to the

1072 sub-arc mantle. Earth Planets and Space, 66, Article Number 61, DOI: 10.1186/1880-
1073 5981-66-61.
1074 Kawamoto, T., Yoshikawa, M., Kumagai, Y., Mirabueno, M.H.T., Okuno, M., and Kobayashi,
1075 T (2013) Mantle wedge infiltrated with saline fluids from dehydration and decarbonation
1076 of subducting slab. Proceedings of the National Academy of Sciences of the United
1077 States of America, 110, 9663-9668.
1078 Kelemen, P.B., Hanghøj, K., and Greene, A.R. (2005) One view of the geochemistry of
1079 subduction-related magmatic arcs, with an emphasis on primitive andesite and lower
1080 crust. In: R.L. Rudnick (ed): Treatise of Geochemistry, Vol. 3: The Crust, 593 – 659
1081 (Elsevier, Amsterdam).
1082 Kelley, K.A., and Cottrell, E. (2009) Water and the oxidation state of subduction zone
1083 magmas. Science, 325, 605-607.
1084 Kent, A.J.R., Peate, D.W., Newman, S., Stolper, E.M., and Pearce, J.A. (2002) Chlorine in
1085 submarine glasses from the Lau Basin: seawater contamination and constraints on the
1086 composition of slab-derived fluids. Earth and Planetary Science Letters, 202, 361-377.
1087 Keppler, H. (1993) Influence of fluorine on the enrichment of high field strength trace
1088 elements in granitic rocks. Contributions to Mineralogy and Petrology, 114, 479-488.
1089 Keppler, H. (1996) Constraints from partitioning experiments on the composition of
1090 subduction-zone fluids. Nature, 380, 237 - 240.
1091 Kessel, R., Schmidt, M.W., Ulmer, P., and Pettke, T. (2005) Trace element signature of
1092 subduction-zone fluids, melts and supercritical liquids at 120–180 km depth. Nature,
1093 437, 724-727.
1094 Kirchbaur, M., and Münker, C. (2015) The behaviour of the extended HFSE group (Nb, Ta,
1095 Zr, Hf,W, Mo) during the petrogenesis of mafic K-rich lavas: The Eastern
1096 Mediterranean case. Geochimica et Cosmochimica Acta, 165,178–199.
1097 Klein-BenDavid, O., Izraeli, E.S., Hauri, E., and Navon, O. (2007) Fluid inclusions in
1098 diamonds from the Diavik mine, Canada and the evolution of diamond-forming fluids.
1099 Geochimica et Cosmochimica Acta, 71, 723–744.
1100 König, S., Münker, C., Schuth, S., and Garbe-Schönberg, D. (2008) Mobility of tungsten in
1101 subduction zone. Earth and Planetary Science Letters, 274, 82-92.

1102 Kumagai, Y., Kawamoto, T., and Yamamoto, J. (2014) Evolution of carbon dioxide-bearing
1103 saline fluids in the mantle wedge beneath the Northeast Japan arc. Contributions to
1104 Mineralogy and Petrology, Article Number: 1056.
1105 Louvel, M., Sanchez-Valle, C., Malfait, W.J., Cardon, H., Testemale, D., Hazemann, J.L.
1106 (2014) Constraints on the mobilization of Zr in magmatic-hydrothermal processes in
1107 subduction zones from in situ fluid-melt partitioning experiments. American
1108 Mineralogist, 99, 1616-1625.
1109 Mallik, A., Nelson, J., and Dasgupta, R. (2015) Partial melting of fertile peridotite fluxed by
1110 hydrous rhyolitic melt at 2-3 GPa: implications for mantle wedge hybridization by
1111 sediment melt and generation of ultrapotassic magmas in convergent margins.
1112 Contributions to Mineralogy and Petrology, 169, Article Number: 48.
1113 Manning, C.E. (1994) The solubility of quartz in H_2O in the lower crust and upper-mantle.
1114 Geochimica et Cosmochimica Acta, 58, 4831-4839.
1115 Manning, C. E. (2004) The chemistry of subduction zone fluids. Earth and Planetary Science
1116 Letters, 223, 1 –16
1117 Manning, C.E., Wilke, M., Schmidt, C., and Cauzid, J. (2008) Rutile solubility in albite-H_2O
1118 and $Na_2Si_3O_7$-H_2O at high temperatures and pressures by in-situ synchrotron radiation
1119 micro-XRF. Earth and Planetary Science Letters, 272, 730-737.
1120 Melzer, S., and Wunder, B. (2000) Island-arc basalt alkali ratios: Constraints from phengite-
1121 fluid partitioning experiments. Geology, 28, 583-586.
1122 McGary, R.S., Evans, R.L., Wannamaker, P.E., Elsenbeck, J., and Rondenay, S. (2014)
1123 Pathway from subducting slab to surface for melt and fluids beneath Mount Rainier.
1124 Nature, 511, 338-340.
1125 Métrich, N., and Wallace, P.J. (2008) Volatile abundances in basaltic magmas and their
1126 degassing paths tracked by melt inclusions. Reviews in Mineralogy and Geochemistry,
1127 69, 363-402.
1128 Michael, P. (1995) Regionally distinctive sources of depleted MORB – evidence from trace-
1129 elements and H_2O. Earth and Planetary Science Letters, 131, 301-320.
1130 Peacock, SM (1990) Fluid processes in subduction zones. Science, 248, 329-337.

Pearce, J.A., Stern, R.J., Bloomer, S.H., and Fryer, P. (2005) Geochemical mapping of the Mariana arc-basin system: Implications for the nature and distribution of subduction components. Geochemistry, Geophysics, Geosystems 6, Q07006, doi: 10.1029/2004GC000895

Peate, D.W., Kokfelt, T.F., Hawkesworth, C.J., van Calsteren, P.W., Hergt, J.M., and Pearce, J.A. (2001) U-series isotope data on Lau Basin glasses: the role of subduction-related fluids during melt generation in back-arc basins. Journal of Petrology, 42, 1449-1470.

Plank, T., Cooper, L.B., and Manning, C.E. (2009) Emerging geothermometers for estimating slab surface temperatures. Nature Geoscience, 2, 611 – 615.

Plank, T., and Langmuir, C.H. (1993) Tracing trace-elements from sediment input to volcanic output at subduction zones. Nature, 362, 739-743.

Ponader, C.W., and Brown, G.E. (1989) Rare-earth elements in silicate glass melt systems. 2. Interactions of La, Gd, and Yb with halogens. Geochimica et Cosmochimica Acta, 53, 2905-2914.

Portnyagin, M., Hoernle, K., Plechov, P., Mironov, N., and Khubunaya, S. (2007) Constraints on mantle melting and composition and nature of slab components in volcanic arcs from volatiles (H_2O, S, Cl, F) and trace elements in melt inclusions from the Kamchatka Arc. Earth and Planetary Science Letters, 255, 53-69.

Rüpke, L.H., Phipps Morgan, J., Hort, M., and Connolly, J.A.D. (2004) Serpentine and the subduction zone water cycle. Earth and Planetary Science Letters, 223, 17– 34.

Ruscitto, D.M., Wallace, P.J., and Kent, A.J.R. (2011) Revisiting the compositions and volatile contents of olivine-hosted melt inclusions from the Mount Shasta region: implications for the formation of high-Mg andesites. Contributions to Mineralogy and Petrology, 162, 109-132.

Ryabchikov, I.D., Orlova, G.P., Kalenchuk, G.Y., Ganeyev, I.I., Udovkina, N.G., and Nosik, L.P. (1989) Reactions of spinel lherzolite with H_2O-CO_2 fluids at 20 kbar and 900 ˚C. Geochemistry International, 26, 56-62.

Saal, A.E., Hauri, E.H., Langmuir, C.H., and Perfit, M.R. (2002) Vapour undersaturation in primitive mid-ocean-ridge basalt and the volatile content of Earth's upper mantle. Nature, 419, 451-455.

1161 Schmidt, M.W., and Poli, S. (1998) Experimentally based water budgets for dehydrating slabs
1162 and consequences for arc magma generation. Earth and Planetary Science Letters,
1163 163, 361-379.
1164 Schmidt, M.W., Vielzeuf, D., and Auzanneau, E. (2004) Melting and dissolution of subducting
1165 crust at high pressures: the key role of white mica. Earth and Planetary Science
1166 Letters, 228, 65-84.
1167 Shannon, R.D. (1976) Revised effective ionic-radii and systematic studies of interatomic
1168 distances in halides and chalcogenides. Acta Crystallographica A, 32, 751-767.
1169 Shen, A.H., and Keppler, H. (1997) Direct observation of complete miscibility the albite-H_2O
1170 system. Nature, 385, 710-712.
1171 Spandler, C., Mavrogenes, J., and Hermann, J. (2007) Experimental constraints on element
1172 mobility from subducted sediments using high-P synthetic fluid/melt inclusions.
1173 Chemical Geology, 239, 228–249.
1174 Spandler, C., and Pirard, C. (2013) Element recycling from subducting slabs to arc crust: A
1175 review. Lithos, 170-171, 208-223.
1176 Stalder, R., Foley, S.F., Brey, G.P., and Horn, I. (1998) Mineral aqueous fluid partitioning of
1177 trace elements at 900-1200 ˚C and 3.0-5.7 GPa: New experimental data for garnet,
1178 clinopyroxene, and rutile, and implications for mantle metasomatism. Geochimica et
1179 Cosmochimica Acta, 62, 1781-1801.
1180 Stolper, E., and Newman, S. (1994) The role of water in the petrogenesis of Mariana trough
1181 magmas. Earth and Planetary Science Letters, 121, 293-325.
1182 Syracuse, E.M., van Keken, P.E., and Abers, G.A. (2010) The global range of subduction
1183 zone thermal models. Physics of the Earth and Planetary Interiors, 183, 73-90.
1184 Sverjensky, D.A., Harrison, B., and Azzolini, D. (2014) Water in the deep Earth: The dielectric
1185 constant and the solubilities of quartz and corundum to 60 kb and 1200 ˚C. Geochimica
1186 et Cosmochimica Acta, 129, 125-145.
1187 Tang, M, Chen, K., and Rudnick, R.L. (2016) Archean upper crust transition from mafic to
1188 felsic marks the onset of plate tectonics. Science, 351, 372-375.
1189 Tatsumi, Y (1989) Migration of fluid phases and genesis of basalt magmas in subduction
1190 zones. Journal of Geophysical Research, 94, 4697-4707.

1191 Tropper, P., and Manning, C.E. (2005) Very low solubility of rutile in H_2O at high pressure and
1192 temperature, and its implications for Ti mobility in subduction zones. American
1193 Mineralogist, 90, 502-505.
1194 Tropper, P., Manning, C.E., and Harlov, D. E. (2011) Solubility of $CePO_4$ monazite and YPO_4
1195 xenotime in H_2O and H_2O–NaCl at 800 °C and 1 GPa: Implications for REE and Y
1196 transport during high-grade metamorphism. Chemical Geology, 282, 58-66.
1197 Tsay, A., Zajacz, Z., and Sanchez-Valle, C. (2014) Efficient mobilization and fractionation of
1198 rare-earth elements by aqueous fluids upon slab dehydration. Earth and Planetary
1199 Science Letters, 398, 101-112.
1200 Turner, S., and Foden, J. (2001) U, Th and Ra disequilibria, Sr, Nd and Pb isotope and trace
1201 element variations in Sunda arc lavas: predominance of a subducted sediment
1202 component. Contributions to Mineralogy and Petrology, 142, 43-57.
1203 Turner, S.J., and Langmuir, C.H. (2015) What processes control the chemical composition of
1204 arc front stratovolcanoes? Geochemistry, Geophysics, Geosystems, 16, 1865-1893.
1205 Ulmer, P., and Trommsdorff, V. (1995) Serpentine stability to mantle depths and subduction-
1206 related magmatism. Science, 268, 858-861.
1207 Van Orman, J.A., Grove, T.L., and Shimizu, N. (2001) Rare earth element diffusion in
1208 diopside: influence of temperature, pressure, and ionic radius, and an elastic model for
1209 diffusion. Contributions to Mineralogy and Petrology, 141, 687-703.
1210 Watson, E.B., and Harrison, T.M. (1983) Zircon saturation revisited - temperature and
1211 composition effects in a variety of crustal magma types. Earth and Planetary Science
1212 Letters, 295-304.
1213 Webster, J.D., Vetere, F., Botcharnikov, R.E., Goldoff, B., McBirney, A., and Doherty, A.L.
1214 (2015) Experimental and modeled chlorine solubilities in aluminosilicate melts at 1 to
1215 7000 bars and 700 to 1250 ˚C: Applications to magmas of Augustine Volcano, Alaska.
1216 American Mineralogist, 100, 522-535.
1217 Weingärtner, H., and Franck, E.U. (2005) Supercritical water as a solvent. Angewandte
1218 Chemie International Edition, 44, 2672-2692.

1219 Weiss, Y., McNeill, J., Pearson, D.G., Nowell, G.M., and Ottley, C.J. (2015) Highly saline
1220 fluids from a subducting slab as the source for fluid-rich diamonds. Nature, 524, 339-
1221 342.
1222 Wilke, M., Schmidt, C., Dubrail, J., Appel, K., Borchert, M., Kvashnina, K., and Manning, C.E.
1223 (2012) Zircon solubility and zirconium complexation in $H_2O+Na_2O+SiO_2$ +/- Al_2O_3 fluids
1224 at high pressure and temperature. Earth and Planetary Science Letters, 349, 15-25.
1225 Wilson, C.A., Spiegelmann, M., van Keken, P. E., and Hacker, B.R. (2014) Fluid flow in
1226 subduction zones: The role of solid rheology and compaction pressure. Earth and
1227 Planetary Science Letters, 401, 261 – 274.
1228 Woodhead, J.D., Hergt, J.M, Davidson, J.P., and Eggins, S.M. (2001) Hafnium isotope
1229 evidence for `conservative' element mobility during subduction zone processes. Earth
1230 and Planetary Science Letters, 192, 331-346.
1231 Zhang, Z., and Duan, Z. (2005) Prediction of the PVT properties of water over wide range of
1232 temperatures and pressures from molecular dynamics simulation. Physics of the Earth
1233 and Planetary Interiors, 149, 335–354.

1237 **TABLE 1.** A compilation of experimentally determined fluid/mineral partition coefficients for the high field strength elements Nb, Ta, Zr, Hf, and Ti

1238

Mineral	Fluid	Reference	P (GPa)	T (°C)	Nb	Ta	Zr	Hf	Ti
Clinopyroxene	H_2O	Keppler (1996)	0.3	1040	< 0.5				
Clinopyroxene	5 m (Na,K)Cl	Keppler (1996)	0.3	1040	< 0.6	< 0.6	< 0.04		< 0.01
Clinopyroxene	H_2O	Brenan et al. (1995)	2	900	1.7 - 200				
Garnet	H_2O	Brenan et al. (1995)	2	900	11 - 42				
Clinopyroxene	H_2O	Stalder et al. (1998)	3 – 5.7	900 – 1200	4.6 - 12	2.4 – 6.6	1.1 – 6.2	0.7 – 5.4	0.58 – 3.2
Garnet	H_2O	Stalder et al. (1998)	3 – 5.7	900 – 1200	1.6 – 14.2	0.6 – 7.3	0.14 – 3.7	0.15 – 3.2	0.34 – 4.2
Bulk eclogite (garnet + cpx)	H_2O	Kessel et al. (2005)	4	700	0.056	0.018	0.024	0.021	0.025
Bulk eclogite (garnet + cpx)	Silicate-rich “supercritical”	Kessel et al. (2005)	6	900	2.87	1.87	0.42	0.56	0.394
Rutile	H_2O	Brenan et al. (1994)	1 - 2	900 - 1100	0.002 – 0.025	0.0004 – 0.024	0.005	0.01	

1239 All partition coefficients are defined on the basis weight percent (or ppm by weight) ratios

TABLE 2. A compilation of experimentally determined fluid/mineral partition coefficients for the high field strength elements U, Th, Mo, and W

Mineral	Fluid	Reference	P (GPa)	T (°C)	O_2 buffer	U	Th	Mo	W
Clinopyroxene	H_2O	Keppler (1996)	0.3	1040	-	<0.3	7.7		
Clinopyroxene	5 m (Na,K)Cl	Keppler (1996)	0.3	1040	-	36	4		
Clinopyroxene	H_2O	Brenan et al. (1995)	2	900	-	1.6 - 100	0.12 - 1		
Garnet	H_2O	Brenan et al. (1995)	2	900	-	1.1	12		
Bulk eclogite (garnet + cpx)	H_2O	Kessel et al. (2005)	4	700	-	0.143	0.119		
Bulk eclogite (garnet + cpx)	Silicate-rich "supercritical"	Kessel et al. (2005)	6	900	-	4.2	24.5		
Clinopyroxene	H_2O*	Bali et al. (2012)	2.6	800-1000	Co-CoO	0.61	0.44	35	3395
Clinopyroxene	H_2O*	Bali et al. (2011, 2012)	2.6	800-1000	Re-ReO_2	1.8	0.84	1076	6870
Clinopyroxene	15 wt % $NaCl_{eq}$	Bali et al. (2011, 2012)	2.6	800-1000	Re-ReO_2	83	1.2	7510	

All partition coefficients are defined on the basis weight percent (or ppm by weight) ratios

* H_2O in this study contains a small amount of NaCl (0.4 wt. %)

1246 **TABLE 3.** A compilation of experimentally determined fluid/mineral partition coefficients for the large-ion lithophile elements Rb, Cs, Sr, Ba, Pb

1247

Mineral	Fluid	Reference	P (GPa)	T (°C)	Rb	Cs	Sr	Ba	Pb
Clinopyroxene	H_2O	Keppler (1996)	0.3	1040	160		0.12	46	1.2
Clinopyroxene	5 m (Na,K)Cl	Keppler (1996)	0.3	1040	1300		2.1	460	58
Clinopyroxene	H_2O	Brenan et al. (1995)	2	900			0.20 – 0.77	1136–2272	19 – 37
Garnet	H_2O	Brenan et al. (1995)	2	900			256 – 2380	30300 – 31250	625 – 833
Clinopyroxene	H_2O	Stalder et al. (1998)	3 – 5.7	900 – 1200			0.7 – 6.5	7 – 42	2 - 27
Garnet	H_2O	Stalder et al. (1998)	3 – 5.7	900 – 1200			9 – 19	6 – 27	1.9 – 27
Bulk eclogite (garnet + cpx)	H_2O	Kessel et al. (2005)	4	700	91	190	0.34	6.1	3.2
Bulk eclogite (garnet + cpx)	Silicate-rich “supercritical”	Kessel et al. (2005)	6	900	310	157	32	65	25.5

1248 All partition coefficients are defined on the basis weight percent (or ppm by weight) ratios

1249

1250 **TABLE 4.** A compilation of experimentally determined fluid/mineral partition coefficients for rare earth elements

1251

Mineral	Fluid	Reference	P (GPa)	T (°C)	La	Ce	Gd	Yb	Lu
Clinopyroxene	H_2O	Keppler (1996)	0.3	1040	< 0.4				
Clinopyroxene	5 m (Na,K)Cl	Keppler (1996)	0.3	1040	1		0.14		0.11
Clinopyroxene	H_2O	Stalder et al. (1998)	3 – 5.7	900 – 1200	0.7 – 5.6	0.5 – 3.4		0.14 – 2.3	
Garnet	H_2O	Stalder et al. (1998)	3 – 5.7	900 – 1200	1.0 – 4.9	0.7 – 4.9		0.0024 – 0.116	
Bulk eclogite (garnet + cpx)	H_2O	Kessel et al. (2005)	4	700	0.28	0.121	0.012	0.005	0.004
Bulk eclogite (garnet + cpx)	Silicate-rich “supercritical”	Kessel et al. (2005)	6	900	17.6	11.8	0.35	0.020	0.017

1252 All partition coefficients are defined on the basis weight percent (or ppm by weight) ratios

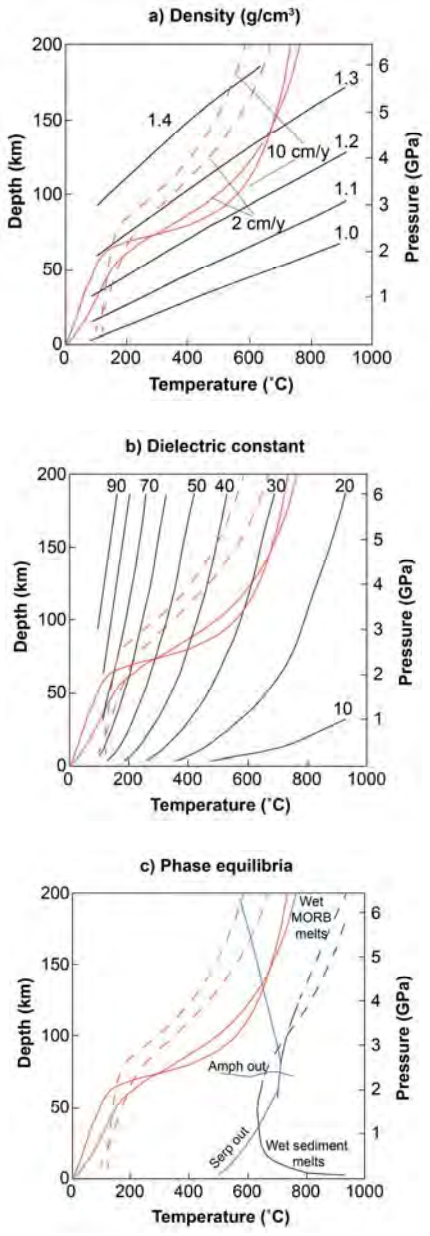

FIGURE 1. Some basic properties of subduction zone fluids. a) Density of water after Zhang and Duan (2005); shown are two geotherms (solid red lines) for the slab surface of 80 Ma old oceanic crust and subduction rates of 2 cm/y and 10 cm/y (after Rüpke et al. 2004); dashed red lines give the temperature at a depth of 8 km below the slab surface. b) Dielectric constant of pure water after Sverjensky et al. (2014). c) Some phase equilibria under water-saturated conditions: Stability limit of serpentine in peridotite (Ulmer and Trommsdorf 1995) and of amphibole in MORB (Schmidt and Poli 1998); water-saturated solidi for MORB (schmidt and Poli 1998) and sediment (Schmidt et al. 2004).

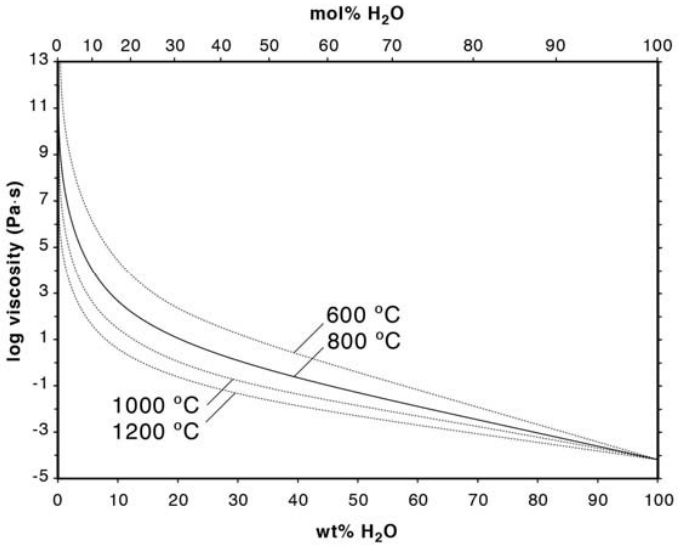

FIGURE 2. Viscosity of subduction zone fluids in H_2O-silicate systems (after Audetat and Keppler 2004). The model was calibrated mostly for the albite ($NaAlSi_3O_8$)-H_2O system at 1 – 2 GPa. However, it likely can also be used for other silicate-H_2O systems and at higher pressures. The conversion of wt% to mol% is based on a model with one oxygen atom per formula unit for each component.

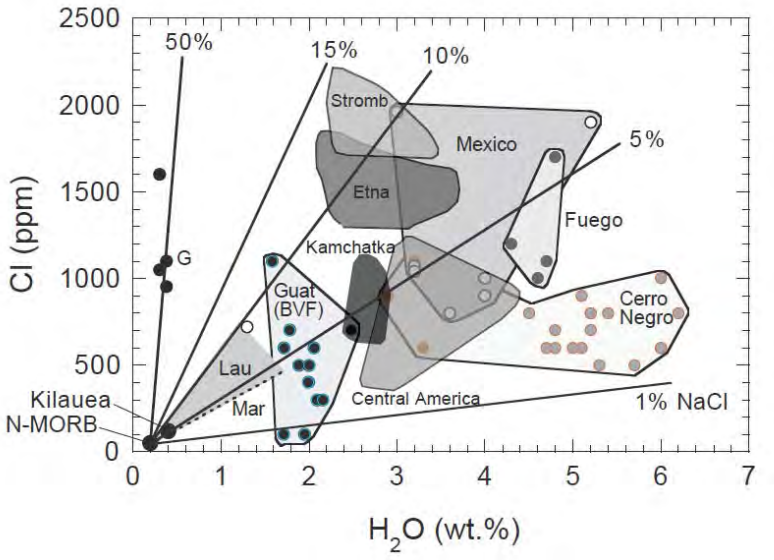

FIGURE 3. H_2O and Cl contents in olivine-hosted melt inclusions from arc basalts. Reproduced from Métrich and Wallace (2008) with permission of MSA. G = Galungung, Indonesia, Guat (BVT) = Guatamalan volcanoes behind volcanic front; Lau = Lau basin; Mar = Mariana trough basalts (dashed line); Stromb = Stromboli, Italy. Lines give the weight percentage of NaCl in aqeous fluids required to produces the observed Cl/H_2O ratios.

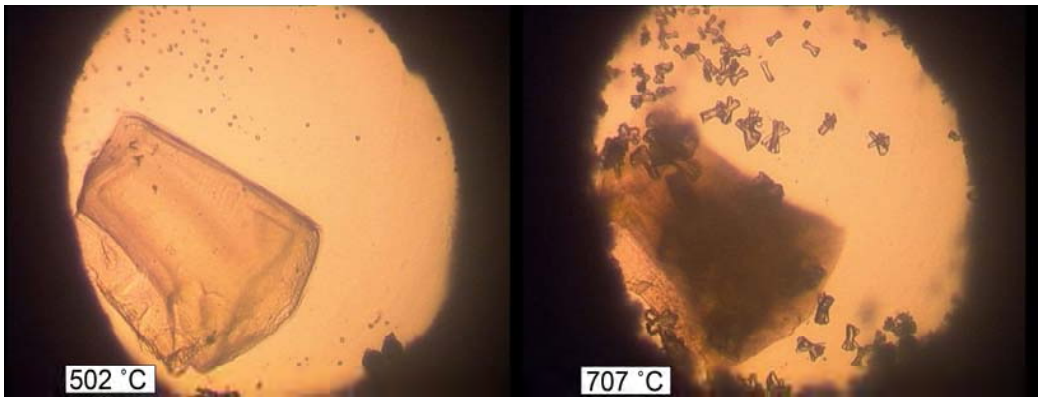

FIGURE 4. Dissolution of a piece of andesitic glass in water as seen during heating in an externally heated diamond cell. Pressure is about 0.65 GPa at 502 ℃ and 0.77 GPa at 707 ℃. The dissolution of the metastable andesite glass produces an oversaturated solution that later causes the precipitation of (not identified) bone-shaped crystals in the entire sample chamber. This illustrates a potential danger in measuring fluid compositions using diamond traps in conventional quench-experiments. If a metastable phase, such as a glass, is used as starting material, super-saturated solutions will be produced that may precipitate crystalline phases in the diamond trap. Upon later analysis of the material in the trap, these crystals will be misidentified as a fluid component. Image courtesy of Andreas Audetat.

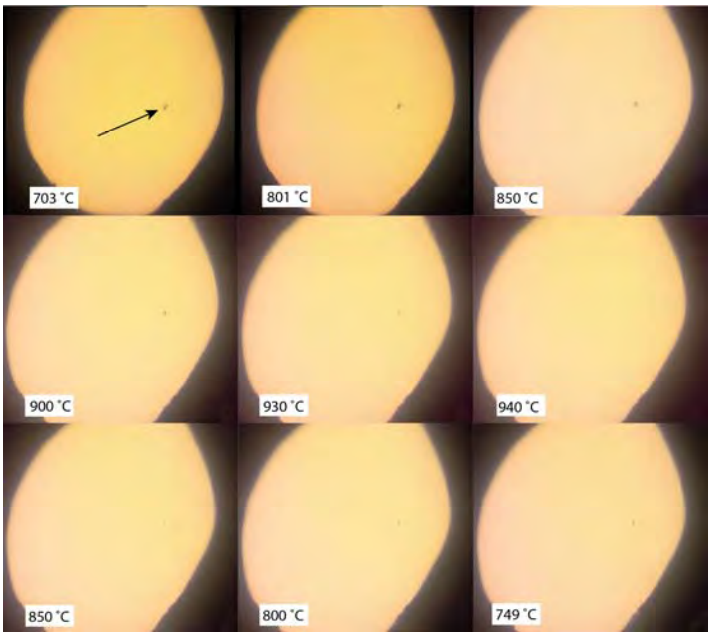

FIGURE 5. Dissolution an re-precipitation of rutile (TiO_2) as seen in an externally-heated diamond cell. The crystal can be seen to dissolve with increasing temperature and to grow again during cooling, demonstrating attainment of equilibrium. Some of the reprecipitation occurs on the gasket (out of focal plane and therefore not visible in this image). The diameter of the sample chamber shown is about 450 μm. Image courtesy of Andreas Audetat.

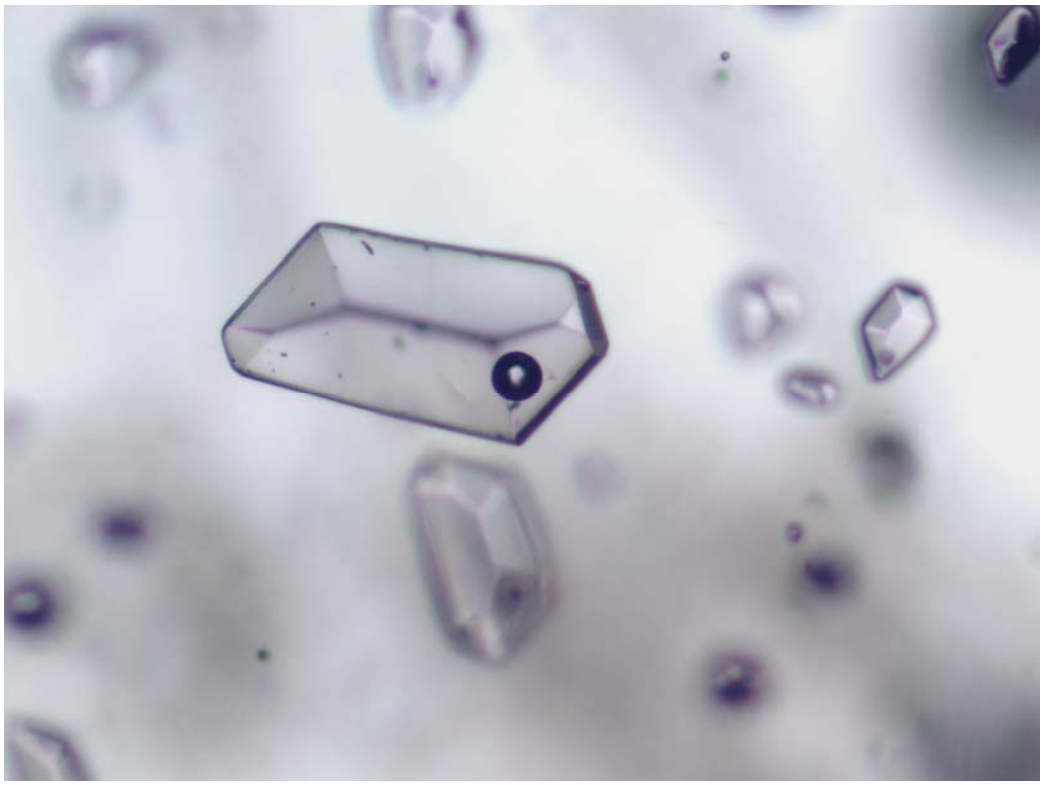

FIGURE 6. Synthetic fluid inclusions in quartz used to determine the solubility of UO_2 in aqueous NaCl-bearing fluids at 1.5 GPa and 800 °C (run 72 of Bali et al. 2011). Note the dark precipitates of UO_2 in the large inclusion (size about 100 μm).

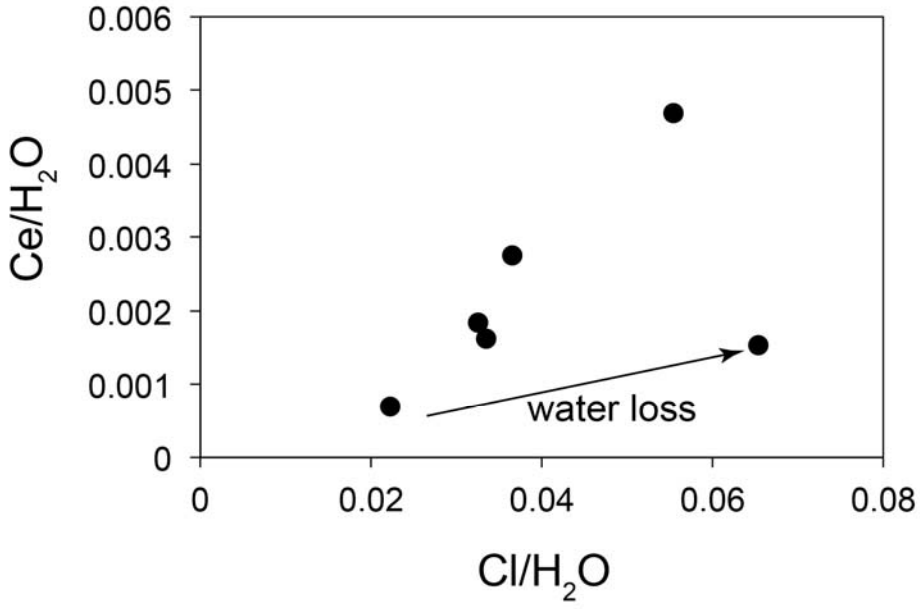

FIGURE 7. The Ce/H_2O ratio from high-Mg basalt melt inclusions in Central Mexico plotted against the Cl/H_2O ratio. The data suggest that fluid transport of Ce was enhanced by high salinity. Data from Cervantes and Wallace (2003). The one inclusion that falls off the main trend may have lost some water after entrapment, which would move the data point on a straight line away from the origin.

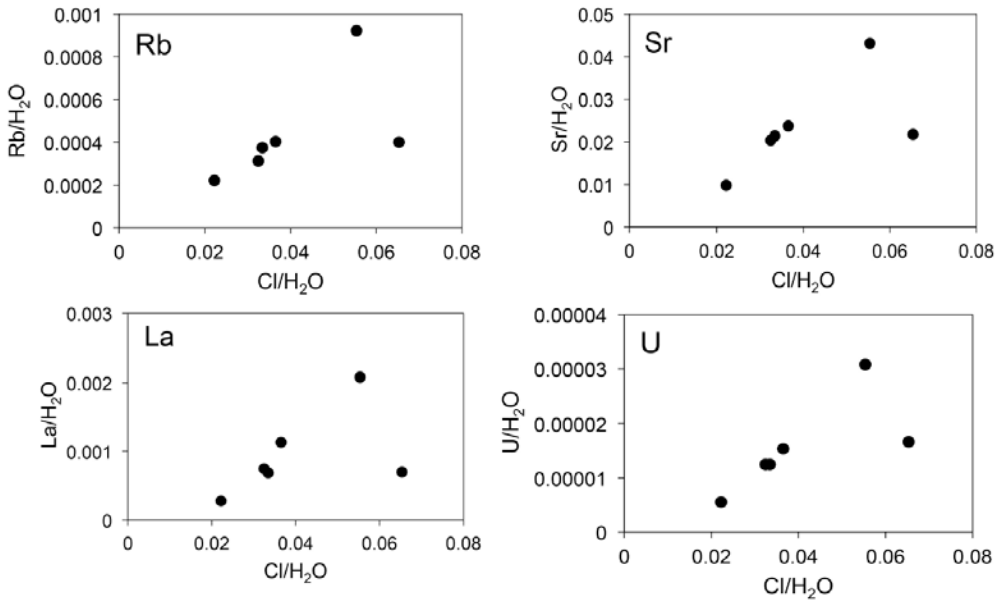

1338

1339 **FIGURE 8.** Abundances of Rb, Sr, La, and U normalized to water as a function of Cl/H_2O in

1340 high-Mg basalt melt inclusions in Central Mexico. The data suggest that fluid transport of

1341 these trace elements was enhanced by high salinity. Data from Cervantes and Wallace

1342 (2003). The one inclusion that falls off the main trend may have lost some water after

1343 entrapment.

1344

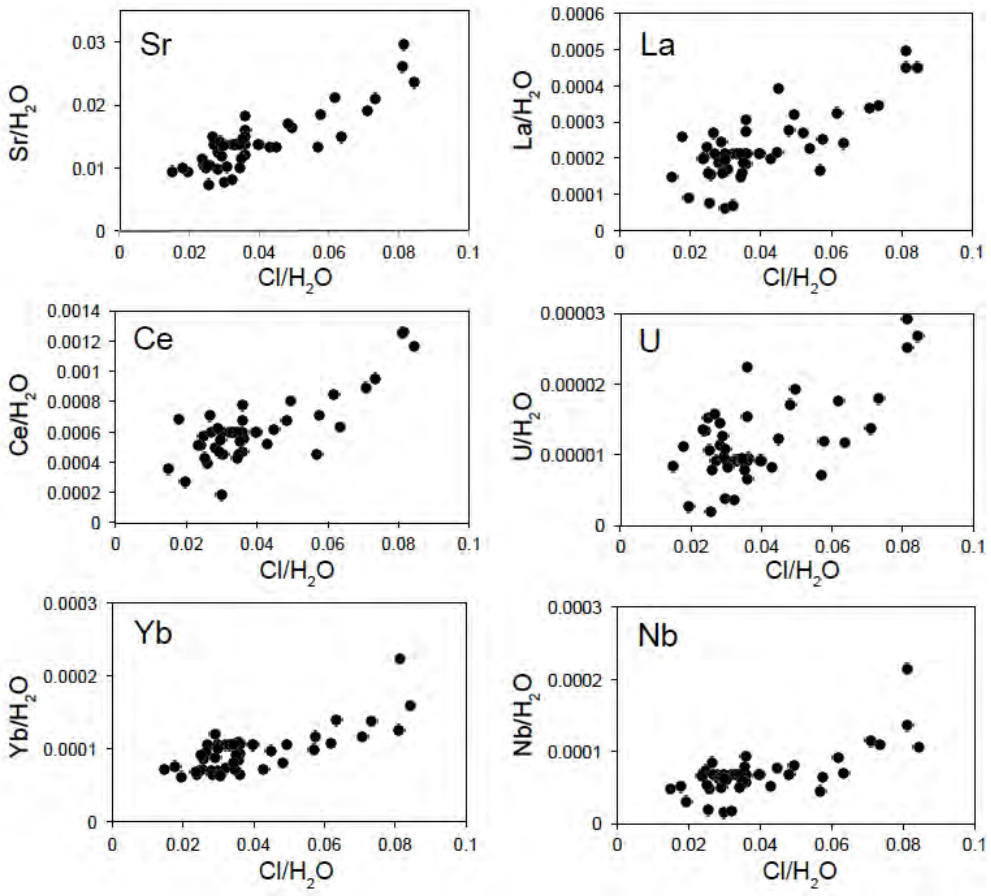

FIGURE 9. Abundances of Sr, La, Ce, U, Yb, and Nb normalized to water as a function of Cl/H_2O in basaltic melt inclusions from Kamchatka. Data from Portnyagin et al. (2007) and the georoc database (georoc.mpch-mainz.gwdg.de).The data suggest that fluid transport of Sr, La, Ce, and U was enhanced by high salinity. The large scatter in the data for uranium may reflect variations in ambient oxygen fugacity. Yb and Nb may only be slightly mobile in the fluid at the highest salinities.